

FORMING CHONDRULES IN IMPACT SPLASHES II VOLATILE RETENTION

CORNELIS PETRUS DULLEMOND, DANIEL HARSONO, SEBASTIAN MARKUS STAMMLER

Institute for Theoretical Astrophysics, Heidelberg University, Albert-Ueberle-Strasse 2, 69120 Heidelberg, Germany

ANDERS JOHANSEN

Lund Observatory, Department of Astronomy and Theoretical Physics, Lund University, Box 43, 22100 Lund, Sweden

Draft version August 12, 2016

ABSTRACT

Solving the mystery of the origin of chondrules is one of the most elusive goals in the field of meteoritics. Recently the idea of planet(esimal) collisions releasing splashes of lava droplets, long considered out of favor, has been reconsidered as a possible origin of chondrules by several papers. One of the main problems with this idea is the lack of quantitative and simple models that can be used to test this scenario by directly comparing to the many known observables of chondrules. In Paper I of this series we presented a simple thermal evolution model of a spherically symmetric expanding cloud of molten lava droplets that is assumed to emerge from a collision between two planetesimals. The production of lava could be either because the two planetesimals were already in a largely molten (or almost molten) state due to heating by ^{26}Al (e.g. Sanders et al. 2005, 2012), or due to impact jetting at higher impact velocities (Johnson et al. 2015). In the present paper, number II of this series, we use this model to calculate whether or not volatile elements such as Na and K will remain abundant in these droplets or whether they will get depleted due to evaporation. The high density of the droplet cloud (e.g. small distance between adjacent droplets) causes the vapor to quickly reach saturation pressure and thus shutting down further evaporation. We show to which extent, and under which conditions, this keeps the abundances of these elements high, as is seen in chondrules. We find that for most parameters of our model (cloud mass, expansion velocity, initial temperature) the volatile elements Mg, Si and Fe remain entirely in the chondrules. The Na and K abundances inside the droplets will initially stay mostly at their initial values due to the saturation of the vapor pressure, but at some point start to drop due to the cloud expansion. However, as soon as the temperature starts to decrease, most or all of the vapor recondenses again. At the end the Na and K elements retain most of their initial abundances, albeit occasionally somewhat reduced, depending on the parameters of the expanding cloud model. These findings appear to be qualitatively consistent with the analysis of Semarkona Type II chondrules by Hewins, Zanda & Bendersky (2012) who found evidence for sodium evaporation followed by recondensation.

Keywords: chondrules, radiative transfer

1. INTRODUCTION

Chondritic meteorites consist for a large part of 0.1 to 1 millimeter size silicate spherules that were once molten lava droplets. These so-called chondrules are much larger than the dust grains in the interstellar medium, and thus must have formed in the protoplanetary disk out of which our solar system was created. So far there is no conclusive evidence as to what was the energy source that produced these 2000 K hot lava droplets. But from the analysis of the textures of these chondrules it is generally concluded that the cooling process was fast: a matter of hours (Hewins et al. 2005; see also references in Morris & Desch 2010). There are abundant theories of what could be the origin of chondrules, among them are nebular shocks (e.g. Hood & Horányi, 1991; Desch & Connolly 2002; Ciesla & Hood 2002; see also Stammer & Dullemond 2014), nebular lightning (Horányi et al. 1995; Eisenhour & Buseck 1995; Gibbard et al. 1997); the X-wind model (Shu et al. 2001) and flash heating by energy dissipation in current sheets forming in MHD turbulence (Hubbard et al. 2012). There are energy conservation analyses showing that the required energy is a

non-negligible fraction of the accretion energy of the protoplanetary disk (King & Pringle 2010). Finally, Jacquet et al. (2012) include mixing processes within the disk in their analysis to see how chondrules produced in different locations disperse and form chondrites.

The alternative theory that chondrules might have originated as a result of planetesimal collisions producing a splash of molten droplets that cooled down to become chondrules (e.g. Urey 1953; Kieffer 1975; Zook 1980) has long been dismissed. However, recently interest in this idea has been revived (Sanders & Taylor 2005; Hevey & Sanders 2006; Asphaug et al. 2011; Sanders & Scott 2012; Fedkin et al. 2012; Fedkin & Grossman 2013; Johnson et al. 2015). One of the main problems with the planetesimal collision scenario is that it takes large impact velocities ($\gtrsim 3 \cdots 5$ km/s) to generate enough impact heat to melt the rock out of which the planetesimals are made. During the gas-rich phases of the protoplanetary disk (lasting a few million years) one would expect that due to friction with the gas the planetesimals have only small eccentricities and inclinations, and thus would collide at much slower speeds, meaning that no melt is produced.

Zook (1980) argued that this problem can be solved if one takes into account that short-lived radionuclides (in particular ^{26}Al) can heat up planetesimals of $\gtrsim 10$ km radius beyond the solidus temperature, essentially turning them into spheres of magma with a crust (Hevey & Sanders 2006; Sanders & Scott 2012). A collision would release the magma into a spray of lava droplets, even if the collision speed is moderate. Asphaug et al. (2011) argued that one can calculate the droplet radius to be consistent with observed sizes if the planetesimals are at least 10 km or more in size.

A potential problem with the pre-molten planetesimals is that they might differentiate if the melting is sufficient, the gravity strong enough and convective mixing not efficient enough. This would mean that the melt they would release would be very non-solar. Recently Johnson et al. (2015) therefore revisited the original high-impact-speed idea in which the cloud of droplets is caused by “impact jetting”. In this model, initially studied in this context by Kieffer (1975), pre-melting is not necessary since the impact velocity is high enough to create the melt through shock-heating at the interface between the colliding bodies. The produced melt will then, under high pressure, escape as a sheet of “jets” to the side. Johnson et al. show that for realistic collision velocities of about 3 km/s only a small fraction of the mass of the impacting bodies ends up in a jet, essentially implying that chondrules are merely a by-product of colliding planets. They calculate, using Monte Carlo calculations of planetesimal populations including the effect of eccentricity damping by the nebular gas, that nevertheless a sufficient number of collisions would occur to account for the total mass in chondrules in the asteroid belt.

Either way (pre-melting or high-velocities), the impact origin of chondrules is being re-investigated. A problem with testing the impact hypothesis is that quantitative models of the splash are scarce, because the process is so complex (see e.g. Asphaug et al. 2011 and Johnson et al. 2015 for hydrodynamic simulations), making it very hard to make quantitative model predictions for quantities such as cooling times and volatile element retention, which are the kind of data that are obtained from meteoritic studies.

In a previous paper we tried to remedy this by presenting a very simple model of a spherically symmetric ballistically expanding cloud of hot lava droplets that radiatively cool through time-dependent radiative transfer (Dullemond, Stammler & Johansen 2014, henceforth Paper I). This thermal model provides droplet number densities and temperatures as a function of time and location within the cloud. In the present paper we will use this model to make model predictions for the abundances of volatile elements in chondrules, and compare this to generic properties of these abundances in chondrites.

The reason for focusing on volatile elements is because the abundances of volatile elements such as Na and K in most chondrules is fairly close to solar (see e.g. Fedkin & Grossman 2013 for a discussion). This is surprising given the high temperatures needed to melt rock to form lava. A millimeter-size lava droplet in vacuum at a temperature of ca. 2000 K would evaporate and lose its Na and K within less than a minute. The fact that we do not see strong depletion of these elements in most chondrules

suggests that the chondrules were at those high temperatures only extremely briefly (tens of seconds at most), suggesting rapid heating and subsequent rapid cooling of the chondrules. This appears to be inconsistent with constraints on cooling rates, which suggest cooling times of the order of hours. Moreover, if evaporation was efficient, one would expect strong isotopic fractionation to occur, which is not observed in chondrules (Cuzzi & Alexander 2006).

A very natural way to prevent the loss of volatile elements is, however, if the chondrules are very close together during their high-temperature formation phase: each chondrule will then have only a limited volume of “private” vacuum around it in which it can outgas its volatiles, and the vapor will then quickly reach saturation pressure. Or in other words: a chondrule will absorb what another nearby chondrule will evaporate. This idea was proposed by Cuzzi & Alexander (2006) and Alexander et al. (2008) to explain the lack of volatile element depletion and fractionation in chondrules. They conclude that chondrules formed a very dense cloud of hundreds of kilometers across before the chondrules cooled down and became solid. Such high-density clouds of solids are not unnatural in protoplanetary disks. For instance, the streaming instability has been shown to produce extremely high concentrations of solids (Johansen & Youdin 2007). It is, however, very hard to imagine any nebular scenario (processes happening in the gas-and-dust protoplanetary disk) which could heat up a large and very dense cloud of proto-chondrules to temperatures of ~ 2000 K in a matter of minutes to hours. The density of such a cloud would be much larger than the gas density of the protoplanetary disk, so that the gas of the disk would not likely be able to release enough energy in a short enough time to heat the proto-chondrules from nebular temperatures (few hundred Kelvin) to melting temperature (ca 2000 K).

Fedkin & Grossman (2012), Hewins, Zanda & Bendersky (2012) and Fedkin et al. (2013) also analyzed the vapor saturation scenario and concluded that impact splashes, in which droplets of molten lava are ejected from an impact event, are the most natural scenario to create these high-density, high-temperature, short-lived environments.

It is the purpose of this series of papers to test this idea with a simple model of a ballistically expanding cloud of droplets that cools through emission of infrared radiation (Paper I). Here (Paper II) we add an evaporation/condensation model to it, but we deliberately keep this evaporation/condensation model simple. The geo/cosmochemical problem of evaporation/condensation of minerals is actually quite complex, and the above mentioned papers treat this in a much more detailed way. Our simplified treatment aims merely at investigating whether the general scenario is feasible, given a ballistically expanding cloud of droplets.

We find that as the cloud of hot lava droplets moves away from the impact site and expands, the vapor quickly reaches saturation pressure. If the cloud is large enough then the vapor diffusion time scale would be larger than the expansion time so that during the expansion process the vapor is not escaping. The total amount of volatile elements in the vapor phase is initially much less than the amount that remains in the solid phase, but under

some conditions shortly before the radiative cooling sets in, a non-negligible fraction of the volatile elements are in the gas phase. As the cloud then cools, the vapor will recondense onto the chondrules. Before the expanding cloud becomes too tenuous for recondensation to be effective all the volatiles have recondensed.

The structure of this paper is as follows. For details on the thermal model we refer to Paper I, but we will give a very brief summary in Section 2. Then we will discuss the time-dependent evaporation and condensation model in Section 3, which is a simplified version of a more detailed model described in the appendices A, B C and D. In this section we also describe the results. Finally in Section 4 we will discuss the results and come to a conclusion.

2. EXPANDING CLOUD MODEL

The goal of the simple model of Paper I was to compute the density and temperature of the cloud of lava droplets as a function of time after the planetesimal collision. The dynamics was assumed to be extremely simple: a spherically symmetric homogeneous cloud expanding with a constant rate while it is moving away from the impact site. The radius of the cloud is thus a linear function of time t since the collision:

$$R_{\text{cloud}}(t) = v_{\text{exp}} t \quad (1)$$

where v_{exp} is the expansion velocity of the cloud. The density of chondrules in the cloud is then

$$\rho_{\text{cloud}}(t) = \frac{3M_{\text{cloud}}}{4\pi R_{\text{cloud}}^3(t)} \quad (2)$$

where M_{cloud} is the total mass of all chondrules in the cloud. The temperature of the lava droplets declines with time as soon as they can radiatively cool. However, right after the onset of expansion the cloud is still very optically thick, meaning that the radiation cannot escape the cloud fast enough. The temperature thus initially stays constant. Only after some time t_{cool} the optical depth drops below some critical value (which is still well above unity) below which the radiative diffusive energy loss kicks in and the temperature starts to drop. In Paper I we calculated this time-dependent radiative cooling numerically with a time-dependent radiative transfer algorithm. We found that these numerical results can be understood and fitted with a simple analytic model. We briefly describe the model here, and refer to Paper I for details. We consider chondrules (lava droplets) of radius a_{chon} and material density ξ_{chon} . We take $\xi_{\text{chon}} = 3.3 \text{ g/cm}^3$ for our model. The mass of a chondrule is then $m_{\text{chon}} = \frac{4\pi}{3}\xi_{\text{chon}}a_{\text{chon}}^3$. The number density of chondrules is $n_{\text{chon}}(t) = \rho_{\text{cloud}}(t)/m_{\text{chon}}$. With the simplifying assumption of zero albedo the absorption opacity is then $\kappa = \frac{3}{4}(\xi_{\text{chon}}a_{\text{chon}})^{-1}$ (geometric opacity). The optical depth from the center of the cloud to the edge is $\tau(t) = \rho_{\text{cloud}}(t)\kappa R_{\text{cloud}}(t)$.

In this paper we will present our results based on a set of fiducial models as well as parameter scans. The parameters of the fiducial models are listed in Table 1. Note that instead of using M_{cloud} as the parameter determining the amount of mass in the cloud of droplets, we instead use $R_{\text{melt},0}$: the equivalent radius of a sphere

Model	$R_{\text{melt},0}$	v_{exp}	T_0	t_{cool}
F1	1 km	100 m/s	2000 K	26 min
F2	0.1 km	1000 m/s	2000 K	16 sec
F3	10 km	100 m/s	2000 K	7 h
F4	0.01 km	1000 m/s	2000 K	1 s

Table 1

The model parameters for the main (“fiducial”) models presented in this paper. The cloud mass M_{cloud} can be derived from

$$M_{\text{cloud}} = \frac{4\pi}{3}\xi_{\text{chon}}R_{\text{melt},0}^3.$$

of melt with mass M_{cloud} , defined through

$$M_{\text{cloud}} = \frac{4\pi}{3}\xi_{\text{chon}}R_{\text{melt},0}^3 \quad (3)$$

Using $R_{\text{melt},0}$ as parameter is more intuitive than M_{cloud} , which is the only reason for using $R_{\text{melt},0}$ instead of M_{cloud} .

In Paper I we found that the temperature of the chondrules at the center of the cloud remains at the initial temperature T_0 for a duration t_{cool} given by:

$$t_{\text{cool}} = \left(\frac{1}{5} \frac{3}{(4\pi)^2} \frac{M_{\text{cloud}}^2 c_m \kappa}{v_{\text{exp}}^4 \sigma T_0^3} \right)^{1/5} \quad (4)$$

where $c_m \simeq 10^7 \text{ erg g}^{-1} \text{ K}^{-1}$ is the specific heat capacity of the chondrule material. For $t > t_{\text{cool}}$ the temperature drops with time. In Paper I it was found that a reasonable analytic description of this temperature decline is:

$$T(t > t_{\text{cool}}) = T_0 \left[\frac{3}{5} \frac{t}{t_{\text{cool}}} + \frac{2}{5} \right]^{-5/3} \quad (5)$$

We assume that for $t < t_{\text{cool}}$ we have:

$$T(t < t_{\text{cool}}) = T_0 \quad (6)$$

The solution Eqs. (5,6) holds true for the central temperature. But most of the mass of a homogeneous sphere resides in the outer parts. For the temperature at $r = 0.8R_{\text{cloud}}$ and $r = 0.9R_{\text{cloud}}$ (roughly the radii of half mass and of 75% mass respectively) the best fitting solution to the full radiative transfer solutions of Paper I are similar to Eq. (5) but with the term $2/5$ replaced by $3/5$ and $3.8/5$ respectively. These analytic estimates of the temperature as a function of time are plotted in Fig. 1, where also the full radiative transfer model results are overplotted. Note that the resulting temperature curves at the center and near the surface of the cloud are qualitatively the same - the only strong difference being the time of onset of the cooling. This means that almost independent of the location within the cloud the chondrule undergo a similarly rapid or slow cooling.

3. TIME-DEPENDENT EVAPORATION/CONDENSATION

Now that we know fairly accurately how the temperature of the cloud declines with time for the given parameters of the model, we will compute the evaporation and condensation process to find out if the chondrules will lose their volatile elements, and if yes, by roughly which amount. The main volatile elements of interest here are Na and K. But we will include other elements such as Fe, Si and Mg mainly as a background reference, since these make up the bulk of the mass of the lava droplet.

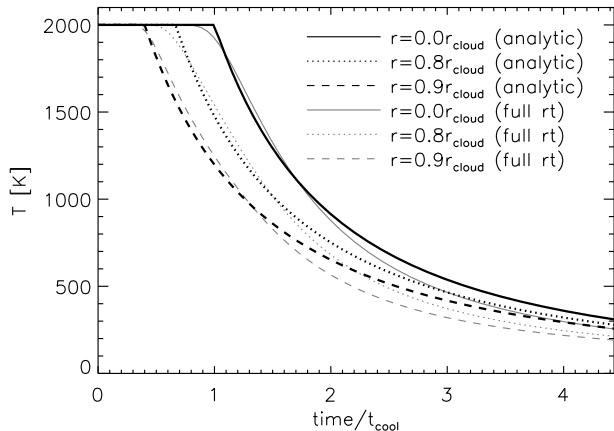


Figure 1. The temperature evolution of the expanding cloud model for the fiducial model F1 (see Table 1). Shown in black are the estimates according to the analytical estimate of Eqs. (5,6). In grey are, for comparison, the full radiative transfer solutions from Paper I. The temperatures are shown at three positions in the cloud: the center, at 80% of the radius and at 90% of the radius (near the surface of the cloud). The time scale is scaled to t_{cool} (Eq. 4). The analytic solutions are only valid as long as the optical depth $\tau_{\text{cool}} \gg 1$.

It should be said that various earlier papers have considered the geochemical problem of evaporation and condensation of Na and K in an impact scenario in much more detail and with much more sophistication than we do here, in particular the paper by Fedkin & Grossman (2013). The main new aspect we focus on here is how this works for the analytic cloud expansion model (Paper I).

Let us consider a volatile material that is initially locked up in the chondrule and might evaporate out of the chondrule when it is hot and liquid. We will focus on Na_2O , K_2O , FeO , SiO_2 and MgO .

In Appendices A, B C and D we describe the evaporation process in detail. We will, however, employ a simplified model of this process for the time-dependent evaporation/condensation modeling which we will describe in Section 3.1. The reason for not employing the full machinery of the evaporation/condensation modeling procedure is that it will qualitatively not change the results much, but it will make the results much less clear and reproducible. Our results are therefore meant to give a rough picture of the process of time-dependent evaporation and condensation of the volatiles in the cloud of lava droplets. This is, at least for now, warranted, because the model is anyway highly simplified, both in the geometry of the cloud as well as in the degree to which laboratory measurements have so far pinned down the detailed time dependent evaporation/condensation behavior under all circumstances. The goal of the present paper is to see how the volatiles behave in the expanding radiatively cooling cloud of droplets. It is *not* the goal to present an evaporation/condensation model per se. For a much more detailed evaporation/condensation model we refer to Fedkin & Grossman (2013).

3.1. A simplified model of time-dependent evaporation/condensation of volatile elements from of lava droplets

Our simplified model is based on the framework described in the appendices A, B C and D. For nomenclature: whenever we talk about “vapor” we mean the volatile element in the gas phase, whereas when we talk about “volatile” we talk about the metal oxide itself (be it in the gas phase or inside the liquid chondrule). We will focus on the volatiles $\text{Na}_2\text{O}(l)$, $\text{K}_2\text{O}(l)$, $\text{FeO}(l)$, $\text{SiO}_2(l)$ and $\text{MgO}(l)$, where (l) stands for the liquid phase. Although these liquid volatiles are predominantly present in the form of $\text{Na}_2\text{SiO}_3(l)$, $\text{KAlSiO}_4(l)$, $\text{Fe}_2\text{SiO}_4(l)$, $\text{SiO}_2(l)$ and $\text{Mg}_2\text{SiO}_4(l)$, we measure the mass weighted abundance f_i of volatile i in terms of the evaporating part of this metal oxide, e.g. for the evaporation of Na_2SiO_3 we measure the mass fraction of Na_2O , because the rest is, upon evaporation, left behind as SiO_2 . We will therefore, from here onward, only refer to Na_2O etc. We assume that the droplet is completely liquid, so that the volatile is always perfectly mixed within the droplet, and no concentration gradients form toward the surface.

In the gas phase (g) the volatiles are present as $\text{Na}(g)$, $\text{K}(g)$, $\text{Fe}(g)$, $\text{SiO}(g)$, $\text{Mg}(g)$ and of course the oxygen $\text{O}_2(g)$ which escapes along with the sodium, potassium, iron, silicon oxide and magnesium. We assume that no other gas is present apart from the vapor itself, i.e. we assume that the nebular gas does not have the chance to enter the cloud before it has cooled down below the solidus. In that case the oxygen pressure follows directly from the partial pressures of the volatile elements (see Eq. B7), so we will focus on Na, K, Fe, SiO and Mg only. The more refractory elements such as Al and Ca are not included in the model because they will not evaporate under the conditions treated in this paper.

From the mass weighted abundance f_i of volatile i (where i is the index of the volatile species: $i = \text{Na}_2\text{O}$, K_2O , FeO , SiO_2 or MgO) we can define the total volatile mass inside the drop:

$$m_{\text{vol},i} = f_i m_{\text{chon}} \quad (7)$$

where m_{chon} is the lava droplet (future chondrule) mass. Since we will see that the most abundant volatiles (SiO_2 , FeO and MgO) evaporate only very little, we can safely assume that the radius a_{chon} will stay approximately constant throughout the simulation.

The rate of evaporation/condensation of a volatile per unit surface area of the lava droplet is given by the Hertz-Knudsen equation (Eq. C1), which in our simplified form reads

$$J_i = \frac{\alpha_i}{\sqrt{2\pi m_{\text{vap},i} k T}} (p_i^{\text{eq}}(f_i, T) - p_i) \quad (8)$$

where $m_{\text{vap},i}$ is the vapor particle mass, k is the Boltzmann constant, α_i is the evaporation/condensation coefficient (the sticking probability of a vapor particle hitting the surface), p_i is the vapor partial pressure, and p_i^{eq} is the equilibrium vapor pressure of vapor species i . The partial pressure of vapor species i is related to the number density n_i of vapor particles via the ideal gas law $p_i = n_i k T$. We assume that the chondrule is completely liquid, so that the volatile elements are always perfectly mixed within the droplet, and no concentration gradients form toward the surface.

In writing down Eq. (8) we made several simplifying assumptions. For one, we assumed that the evaporation and condensation coefficients are equal: $\alpha_{\text{evap},i} = \alpha_{\text{cond},i} \equiv \alpha_i$, and constant under all conditions. We take the values inferred by Fedkin et al. (2006) from their careful fitting of the Hertz-Knudsen equation to the experiments. Their values are approximately $\alpha_{\text{Na}} = 0.26$, $\alpha_{\text{K}} = 0.13$, $\alpha_{\text{Fe}} = 0.23$, $\alpha_{\text{SiO}} \simeq 0.14$ and $\alpha_{\text{Mg}} \simeq 0.26$. Secondly, the computation of the equilibrium vapor pressures p_i^{eq} for all the species is done using the following simplified procedure:

1. Before the start of the simulation we compute the functional form of the equilibrium pressures for the coupled congruent evaporation/condensation problem as a function of temperature, for the given initial composition of the lava droplets (see appendix B). We assume here that a negligible amount of nebular gas is present around the lava droplets, which is a reasonable assumption given that the expanding cloud will be very dense and thus initially “snowplow” the nebular gas. With this assumption the gas between the lava droplets consists 100% of vapor from the lava droplets themselves. For each species we represent this function $p_i^{\text{eq},0}(T)$ by a 3rd order polynomial fit:

$$\log^{10} \left(\frac{p_i^{\text{eq},0}(T)}{10^6 \text{ dyne/cm}^2} \right) = q_{i,0} + q_{i,1} T + q_{i,2} T^2 + q_{i,3} T^3 \quad (9)$$

where 1 bar is 10^6 dyne/cm^2 . The coefficients $q_{i,k}$ for the “composition 3” of Yu et al. (2003) are given in Table 3. During the entire simulation these coefficients $q_{i,k}$ are kept fixed, but when the temperature T varies, the values of $p_i^{\text{eq},0}(T)$ change according to Eq. (9).

2. As the mass fractions f_i of the volatiles vary with time, we assume that their equilibrium pressures vary linearly with f_i :

$$p_i^{\text{eq}}(f_i, T) = \frac{f_i}{f_{0,i}} p_i^{\text{eq},0}(T) \equiv f_i p_i^{\text{eq},00}(T) \quad (10)$$

Here $f_{0,i}$ is the initial value of f_i (i.e. the initial composition of the droplet), and $p_i^{\text{eq},00}(T)$ is defined as $p_i^{\text{eq},00}(T) \equiv p_i^{\text{eq},0}(T)/f_{0,i}$ and the function $p_i^{\text{eq},0}(T)$ is given by Eq. (9). The interpretation of $p_i^{\text{eq},00}(T)$ is the equilibrium vapor pressure if the surface would consist 100% of volatile species i . The linear behavior of Eq. (10) appears to be counter to the expected behavior for Na and K, where p_i^{eq} is expected to be proportional to $\sqrt{f_i}$ (see appendix B). However, in the vacuum evaporation experiments of Yu et al. (2003) an exponential decay of f_i with time appears to be observed for Na and K, which suggests a linear behavior. See the discussion by Alexander (2001). For simplicity we will therefore stick to a linear dependence of p_i^{eq} on f_i as given in Eq. (10). This equation also implies that variations in f_i do not influence $p_{k \neq i}^{\text{eq}}$. Also this is not strictly true, but since our

results show that f_i will never become $f_i \ll f_{0,i}$ this simplification is justified as well.

The loss rate of volatile i from the chondrule is

$$\frac{d(m_{\text{vol},i})}{dt} \equiv \frac{d(f_i m_{\text{chon}})}{dt} \equiv m_{\text{chon}} \frac{df_i}{dt} = -4\pi a_{\text{chon}}^2 J_i m_{\text{vap},i} \quad (11)$$

where we assume that the droplet radius a_{chon} and mass m_{chon} do not change appreciably with time. The time scale of evaporation into vacuum (i.e. assuming that the ambient vapor pressure $p_i = 0$) is then

$$t_{\text{evap},i} \equiv \frac{f_i m_{\text{chon}}}{|d(f_i m_{\text{chon}})/dt|} = \frac{m_{\text{chon}} k T}{4\pi a_{\text{chon}}^2 m_{\text{vap},i} \alpha_i v_i p_i^{\text{eq},00}} \quad (12)$$

where f_i has dropped out of the equation because of the assumed linear scaling between the equilibrium vapor pressure and the mass fraction of the volatile. This means that when the lava droplet resides in vacuum its volatile abundance $f_i(t)$ goes as

$$f_i(t) = f_{0,i} e^{-t/t_{\text{evap},i}} \quad (13)$$

where $f_{0,i}$ is the abundance at $t = 0$.

However, in our expanding chondrule cloud model we must include saturation because the chondrules are very close to each other. We assume that the space between the chondrules is vacuum except for the vapor that just evaporated from the chondrules. Each chondrule has a volume V around it which it can fill up with vapor. The idea here is that if a cloud of chondrules of mass M_{cloud} has a radius of R_{cloud} , then the volume per chondrule is:

$$V = \frac{4\pi}{3} \frac{m_{\text{chon}} R_{\text{cloud}}^3}{M_{\text{cloud}}} \quad (14)$$

which is then the vacuum space that the vapor from each chondrule can fill (where we made the assumption that $V \gg (4\pi/3)a_{\text{chon}}^3$, which is always guaranteed in the parameter range of interest). This assumes, of course, that the vapor will not hydrodynamically flow out of the cloud.

To get a feeling for the numbers it is instructive to use Eq. (14) to define the typical distance d between neighboring chondrules as twice the radius belonging to the volume V (Wigner-Seitz radius):

$$d(t) = 2 \left(\frac{m_{\text{chon}}}{M_{\text{cloud}}} \right)^{1/3} R_{\text{cloud}}(t) \quad (15)$$

This distance increases linearly in time. The neighboring chondrules thus move away from each other at a speed v_{chonseps} given by

$$v_{\text{chonseps}} = \frac{dd(t)}{dt} = 2 \left(\frac{m_{\text{chon}}}{M_{\text{cloud}}} \right)^{1/3} v_{\text{exp}} \quad (16)$$

This v_{chonseps} typically has values of *millimeters per minute*, i.e. these are very low velocities.

At the moment of impact (the start of the expansion of the cloud) we start with a volatile abundances $f_{0,i}$ inside the chondrule. If we know that some time later a volatile abundance f_i is left inside the chondrule then the number density of gas phase vapor particles must be

$$n_i = \frac{(f_{0,i} - f_i) m_{\text{chon}}}{m_{\text{vap},i} V} \quad (17)$$

or equivalently the mass density of vapor particles:

$$\rho_i = \frac{(f_{0,i} - f_i)m_{\text{chon}}}{V} \quad (18)$$

which is independent of the vapor particle mass $m_{\text{vap},i}$.

In equilibrium (i.e. assuming we have infinite time to evaporate and saturate) the vapor number density n_i of species i must be

$$n_i = \frac{p_i^{\text{eq}}(f_i)}{kT} = \frac{f_i p_i^{\text{eq},00}}{kT} \quad (19)$$

By combining this equation with Eq. (17) we can solve for f_i and obtain the equilibrium value for the remaining abundance of the volatile element inside the liquid chondrule:

$$f_{\text{eq},i} = \left(1 + \frac{m_{\text{vap}} V p_i^{\text{eq},00}}{m_{\text{chon}} kT}\right)^{-1} f_{0,i} \quad (20)$$

This is the saturation value of the abundance of the volatile, given the volume V around each chondrule. We can also estimate the volume needed to have 1% or 50% of the volatile in the gas phase. We set $f_{\text{eq},i} = f_{0,i}/100$ or $f_{\text{eq},i} = f_{0,i}/2$ respectively and find

$$V_{1\%} = \frac{m_{\text{chon}} kT}{100 m_{\text{vap},i} p_i^{\text{eq},00}}, \quad V_{50\%} = \frac{m_{\text{chon}} kT}{m_{\text{vap},i} p_i^{\text{eq},00}}. \quad (21)$$

We can find the times $t_{1\%}$ and $t_{50\%}$ when this volume is reached by inserting Eq. (14) into Eq. (21) and solving for t :

$$t_{1\%} = \left(\frac{M_{\text{cloud}} kT}{100 v_{\text{exp}}^3 m_{\text{vap},i} p_i^{\text{eq},00}} \right)^{1/3}, \quad t_{50\%} = \left(\frac{M_{\text{cloud}} kT}{v_{\text{exp}}^3 m_{\text{vap},i} p_i^{\text{eq},00}} \right)^{1/3} \quad (22)$$

The mass loss/gain from/to the chondrule is given by Eq. (11). We can now rewrite Eq. (11) with the equation for the vapor number density Eq. (17), and using the Hertz-Knudsen equation (Eq. 8), into a time-evolution equation for the volatile abundance f_i :

$$\frac{df_i}{dt} = 4\pi a_{\text{chon}}^2 \frac{m_{\text{vap},i} \alpha_i v_i}{m_{\text{chon}}} \left(\frac{(f_{0,i} - f_i)m_{\text{chon}}}{m_{\text{vap},i} V} - \frac{p_i^{\text{eq},00} f_i}{kT} \right) \quad (23)$$

Using Eq. (20) this can be rewritten as

$$\frac{df_i}{dt} = 4\pi a_{\text{chon}}^2 \frac{\alpha_i v_i}{V} \left(1 + \frac{m_{\text{vap},i} V p_i^{\text{eq},00}}{m_{\text{chon}} kT} \right) (f_{\text{eq},i} - f_i) \quad (24)$$

Assuming that between some time t_1 and $t > t_1$ the values of V , T and a_{chon} do not change, the solution is:

$$f_i(t) = f_{\text{eq},i} + (f_i(t_1) - f_{\text{eq},i}) e^{-(t-t_1)/t_{\text{eq},i}} \quad (25)$$

with the equilibration timescale $t_{\text{eq},i}$ given by

$$t_{\text{eq},i} = \left[4\pi a_{\text{chon}}^2 \frac{\alpha_i v_i}{V} \left(1 + \frac{m_{\text{vap},i} V p_i^{\text{eq},00}}{m_i kT} \right) \right]^{-1} \quad (26)$$

As a test, note that for $V \rightarrow \infty$ (evaporation into vacuum, no saturation) we obtain

$$\lim_{V \rightarrow \infty} t_{\text{eq},i} \rightarrow t_{\text{evap},i} \quad (27)$$

where the evaporation time scale $t_{\text{evap},i}$ is given by Eq. (12). For this extreme case we get $\lim_{V \rightarrow \infty} f_{\text{eq},i} \rightarrow 0$ (from Eq. 20), and so solution Eq. (25) then indeed reduces to the time dependent formula for evaporation into vacuum Eq. (13), as expected. For non-infinite V we have $t_{\text{eq},i} < t_{\text{evap},i}$.

In the expanding cloud model of Paper I the temperature changes with time. An analytical approximation to the temperature as a function of time is given, and also the number density of chondrule droplets (or equivalently the volume V around each chondrule) as a function of time is a simple formula. Given that the analytic solution of the volatile abundance $f_i(t)$ of Eq. (25) only strictly holds for constant T and constant V , we cannot simply apply Eq. (25) to the expanding cloud model. However, we can apply Eq. (25) piecewise for each time step, where $f_{0,i}$ is the abundance at the start of the time step (time t_0) and $f_i(t = t_0 + \Delta t)$ is then obtained from Eq. (25). This yields a very stable and easy method of numerical integration of Eq. (24). During every time step we consider T and V constant so that the analytic solution Eq. (25) applies, but for each time step the values of T and V will be different. The full procedure is that at each time step we first calculate the new temperature structure $T(r, t)$, either using the full radiative transfer method of Paper I or by using its analytic approximation. Then we assume that for the entire time step this temperature and the volume V are constant so that we can use Eq. (25) to compute the new abundances. Then we repeat this procedure for the next time step etc.

3.2. Results of the time-dependent evaporation/condensation

As initial composition we take ‘‘composition 3’’ from Yu et al. (2003). These values are listed in Table 2.

The results of fiducial models F1 and F2 (see table 1) are shown in Figs. 2, 3. In Fig. 4 the time-dependent abundance of all volatiles are shown for models F1, F2, F3 and F4. The results show that at very early times ($t \ll t_{\text{cool}}$, well before the cloud temperature starts to drop) the evaporation of all volatiles nearly instantly reaches saturation at the abundance $f_i = f_{\text{eq},i}$ given by Eq. (20). This nearly instant saturation can be seen in Fig. 3 which compares the various time scales with each other for sodium. For early times the equilibration time scale t_{eq} is clearly much smaller than t , so that the equilibrium vapor pressure (and thus the equilibrium abundance) is easily reached within that time. At these early times the corresponding abundance of the volatile inside the lava droplet is nearly identical to the initial abundance ($f_{\text{eq},i} \simeq f_{0,i}$) because the volume per chondrule V is still so small that there is no space to deposit much vapor. In other words: at these early stages hardly any volatile is in vapor form. This can also be seen by looking at the $t_{1\%}$ curve in Fig. 3: only at a relatively late time (10 minutes for model F1 and 0.1 minutes for model F2) will $t_{1\%}$ become smaller than t , or in other words: before $t_{1\%}$ less than 1% of the volatile is in vapor form.

As time progresses and the volume of space around

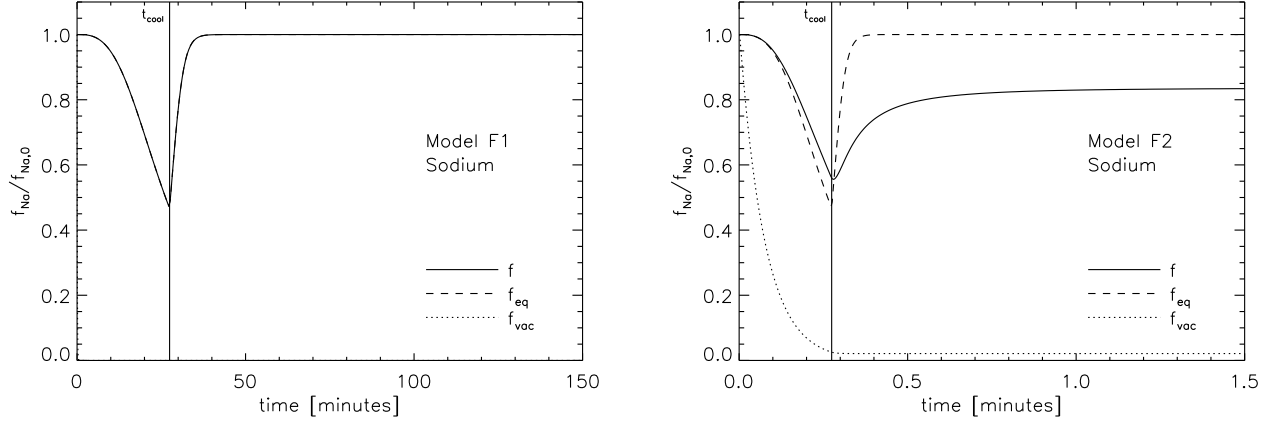


Figure 2. Abundance of Na (relative to the initial abundance) as a function of time for models F1 ($R_{\text{melt},0} = 1 \text{ km}$, $v_{\text{exp}} = 0.1 \text{ km/s}$ - left) and F2 ($R_{\text{melt},0} = 0.1 \text{ km}$, $v_{\text{exp}} = 1 \text{ km/s}$ - right). Here the temperature model is the analytic model of Eqs. (5,6). The solid line is the result of the full evaporation/condensation model. The dashed line is the equilibrium abundance for the given temperature $T(t)$ and volume-per-chondrule $V(t)$ at that time. The dotted line is the abundance if only evaporation is included (no condensation, hence no saturation). The dashed line can only be distinguished in model F2 because in model F1 the dashed and solid lines overlap as a result of the equilibration time t_{eq} (Eq. 26) being very small compared to t in model F1. The dotted line is also hard to find in model F1 because it drops to zero very early on.

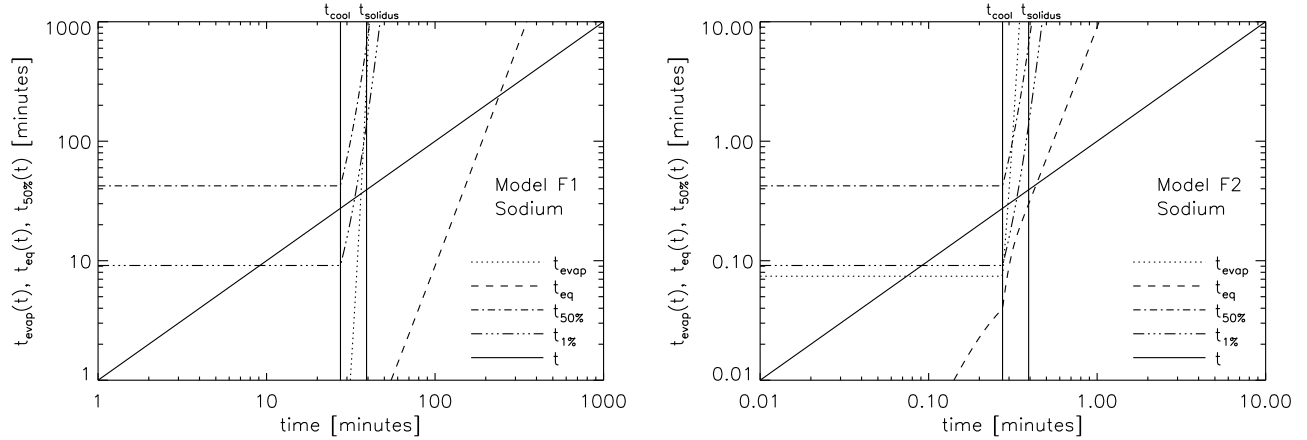


Figure 3. The most important time scales as a function of time for models F1 ($R_{\text{melt},0} = 1 \text{ km}$, $v_{\text{exp}} = 0.1 \text{ km/s}$ - left) and F2 ($R_{\text{melt},0} = 0.1 \text{ km}$, $v_{\text{exp}} = 1 \text{ km/s}$ - right): the evaporation time scale t_{evap} (dotted line), the equilibration time scale t_{eq} , the 50% evaporation time scale $t_{50\%}$ and the 1% evaporation time scale $t_{1\%}$. Here the temperature model is the analytic model of Eqs. (5,6). The time when the temperature drop starts (t_{cool}) and the time when the solidus temperature of 1400 K is reached (t_{solidus}) are marked with vertical lines in the figure. Note that in this figure both axes are logarithmic, in contrast to the other figures.

each chondrule increases, the volatile abundance $f(t)$ inside the chondrules decreases due to evaporation. This is best studied by first looking at the equilibrium abundance $f_{\text{eq},i}(t)$ as a function of time, as shown in Fig. 2 for sodium. It shows that $f_{\text{eq},i}$ drops more and more during the initial constant-temperature phase which lasts until $t = t_{\text{cool}}$, but once the cloud starts to cool down (for $t > t_{\text{cool}}$) it rises again. This is because at low temperatures the vapor wants to recondense onto the chondrules, in spite of the increase of volume per chondrule V . The question is: will the actual abundance $f(t)$ follow the equilibrium abundance $f_{\text{eq},i}(t)$? In other words: can the evaporation/condensation process in this model be approximated by a time-sequence of equilibrium states at ever increasing volume V and decreasing temperature T ? This can be answered by looking again at Fig. 3. In par-

ticular in model F1 one sees that the equilibration time scale t_{eq} for sodium is very much smaller than t until well after t_{cool} . The abundance $f(t)$ thus has no problem following $f_{\text{eq}}(t)$. This explains why in Fig. 2 for model F1 one cannot even distinguish between the curves for $f(t)$ and $f_{\text{eq}}(t)$. This means that while some of the sodium is turned into vapor around $t \simeq t_{\text{cool}}$, the rapid drop in temperature for $t > t_{\text{cool}}$ will cause nearly all of the vapor to recondense back into the droplets. For model F2 (high expansion velocity), however, the equilibration time scale for sodium exceeds t already soon after t_{cool} , and it can be seen in Fig. 2 that $f_i(t)$ and $f_{\text{eq},i}(t)$ start to deviate from each other. The recondensation does not manage to finish before the volume V becomes so big that the recondensation stagnates. This means that some sodium vapor remains in the vapor phase and does not recon-

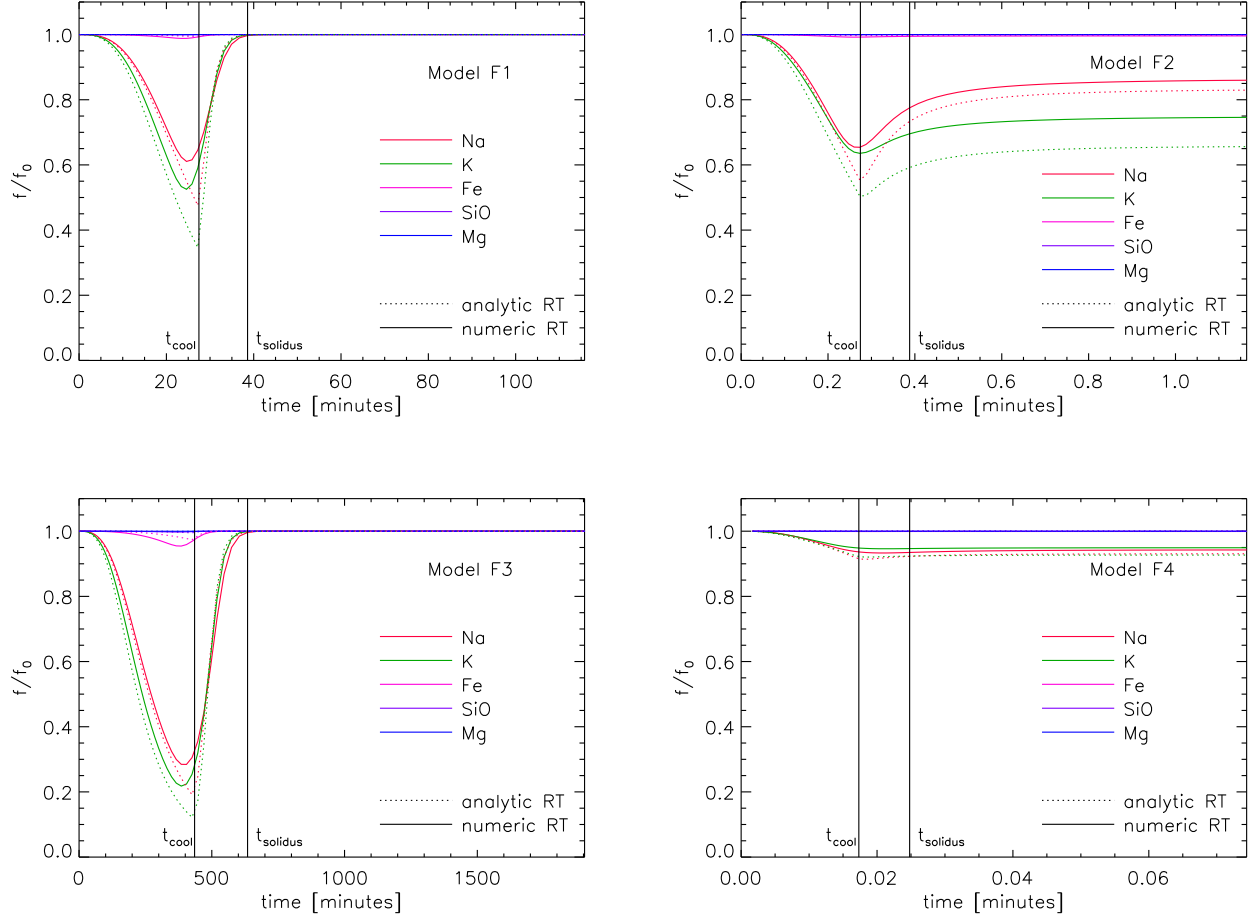


Figure 4. Results of the model F1 ($R_{\text{melt},0} = 1 \text{ km}$, $v_{\text{exp}} = 0.1 \text{ km/s}$), F2 ($R_{\text{melt},0} = 0.1 \text{ km}$, $v_{\text{exp}} = 1 \text{ km/s}$), F3 ($R_{\text{melt},0} = 10 \text{ km}$, $v_{\text{exp}} = 0.1 \text{ km/s}$) and F4 ($R_{\text{melt},0} = 0.01 \text{ km}$, $v_{\text{exp}} = 1 \text{ km/s}$) (left-to-right, top-to-bottom): the abundances of the volatiles as a function of time at the center ($r = 0$) of the cloud. Overplotted are the models when using the analytic temperature solution (dotted) and the full radiative transfer temperature solution (solid).

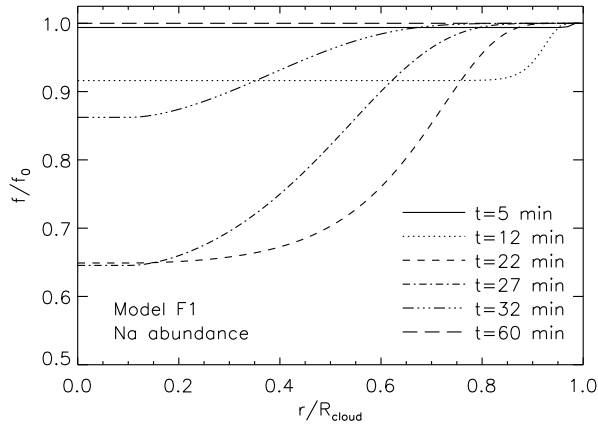


Figure 5. Result of model F1 ($R_{\text{melt},0} = 1 \text{ km}$, $v_{\text{exp}} = 0.1 \text{ km/s}$) for Na, plotted as a function of $\eta = r/R_{\text{cloud}}$ for several time instances.

dense, and thus some sodium is lost permanently from the chondrules for model F2. This behavior can not be modeled by a sequence of equilibrium models, and is a

clear case of time-dependent non-equilibrium evaporation/condensation. One is now compelled to ask: what will happen to this non-condensed vapor? This is not trivial to answer and will depend on when the simple ballistically expanding cloud model will break down. A reasonable scenario is that once the chondrules and the remaining vapor dissipate into the solar nebula, the vapor will condense out onto the fine-grained dust in the nebula. In other words: the chondrules would then be somewhat depleted in these volatiles, while the fine-grained nebular dust (which is perhaps the future matrix?) will be enhanced in these volatiles.

Fig. 4 shows the abundances of all five volatiles as a function of time for all models. Both the full radiative transfer temperature model as well as the analytic temperature model of Eqs. (5,6) are shown, and they agree very well. In model F1, the model with an intermediate expansion velocity, all volatiles recondense back onto the chondrules. We thus expect that for these parameters no volatile losses should be found in chondrules (modulo possible hydrodynamic escape effects). For model F2, the model with a high expansion velocity (1 km/s), the volatile losses are considerable, at least for Na and K. The elements Mg and Si seem to be entirely immune to

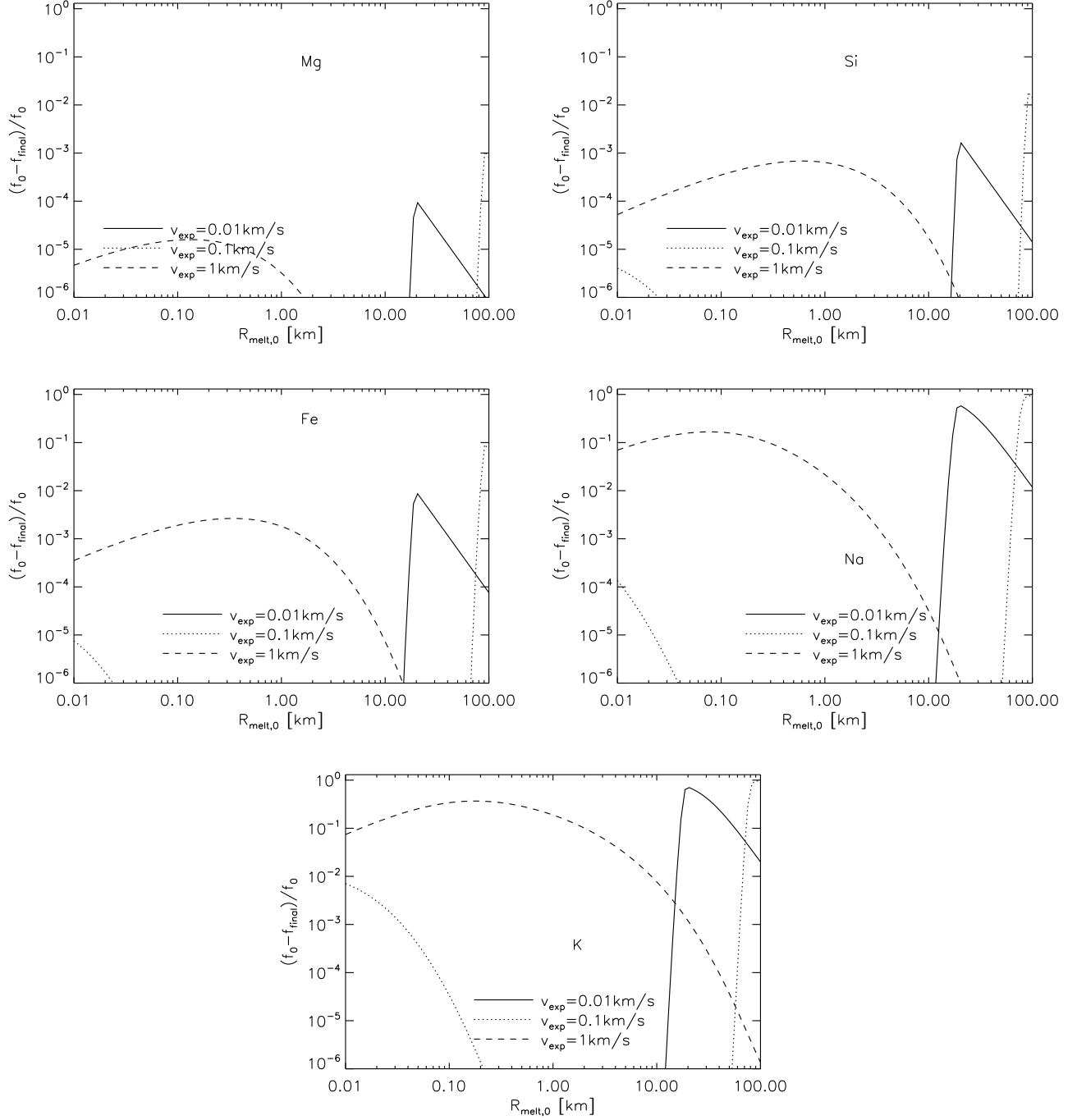


Figure 6. The fraction of volatiles that are lost from the droplets at the end of the expansion of the cloud. Plotted is $(f_0 - f(t \rightarrow \infty))/f_0$ (where f_0 is the initial fraction of volatiles in the melt) as a function of the initial mass of the cloud expressed in terms of the equivalent radius $R_{\text{melt},0}$ (cf. Eq. 3) for three values of the expansion velocity v_{exp} . The analytic temperature model was used.

evaporation under these conditions, while Fe does appear to be slightly affected for model F2.

The models show that if it were not for the high density of the cloud, the sodium and potassium would have been almost completely lost from the chondrules. That vapor would then have dispersed into the nebula and much later would have recondensed onto the fine-grained nebular dust. The “savior” of the volatiles is the fact that the expanding cloud of lava droplets reaches its cooling

time $t = t_{\text{cool}}$ typically before the moment when equilibration time $t_{\text{eq},i}$ drops below t . That means that if some volatiles may have vaporized during the expansion, the temperature will drop soon enough for the vapor to recondense onto the chondrules before the vapor would be lost. Moreover, for Fe, SiO and Mg most of the volatile elements never even reach the gas phase because before $t = t_{\text{cool}}$ the available volume per chondrule is still too small to be able to store much of the volatile element

in vapor form. Only for Na and K there is a moment (around $t = t_{\text{cool}}$) where most of the volatile is in vapor form. However, soon after t_{cool} , as the temperature drops, some (model F2) or all (model F1) of the vapor recondenses again.

Model F3 is a model of a very massive and slowly expanding cloud. Interestingly for this model the volatile abundances reach the lowest intermediate values of all models before returning completely back to their original values. This may appear counter-intuitive, as we expect the slow expansion to keep the volume around each chondrule small for a long time. The essential time scale, however, is the time at which the cooling starts. If the volume around each chondrule reaches large enough values for most of the volatile to escape the lava droplets before the cooling sets in, then the depletion at $t = t_{\text{cool}}$ will be the largest.

Model F4 is the most extreme one, where the cloud expands so fast that any volatiles lost until $t = t_{\text{cool}}$ will not have the time to recondense before the cloud has essentially dispersed. The lost vapor will then presumably recondense out on nebular dust grains.

The results of all models do depend somewhat on position within the cloud. The results shown so far are for the center of the cloud. Toward the edge of the cloud the cooling sets in earlier, and hence also the recondensation. Fig. 5 shows, as an example, the radial dependence within the cloud of the Na-abundance in model F1 for several time snapshots. As radial coordinate the dimensionless $\eta = r/R_{\text{cloud}}$ is used, so that the edge of the cloud is, at each time snapshot, located at the same position $\eta = 1$. In other words: that the results are all shown at the same relative spatial scales. One sees that the strongest depletion occurs at intermediate times in the center of the cloud, whereas toward the edge less depletion occurs. This is because the outer regions of the cloud are cooler, and therefore the equilibrium vapor pressure is lower.

It is interesting to investigate how much of the vapor still recondenses after the solidus temperature is reached. This vapor would then produce a layer of high concentration of the element around the chondrule. Any vapor that recondenses shortly before the solidus is reached may still partly diffuse into the chondrule but perhaps not perfectly, predicting that that volatile element would have a higher concentration near the surface of the chondrule than near the center. The time of reaching the solidus temperature is marked in Fig. 4.

Fig. 6 shows the final results of the models: the fraction of volatiles permanently lost from the chondrules at the end of the models for various cloud masses and expansion velocities. This shows that strong losses are only expected for extremely high expansion velocities ($\gtrsim 1$ km/s), or for very massive ($R_{\text{melt},0} \gtrsim 10$ km) but slowly expanding clouds. This opens the possibility that measurements of the degree of volatile loss can distinguish between low and high velocity impacts and/or large or small vapor cloud masses. All these results are, however still without taking into account the hydrodynamic loss of the volatile.

3.3. Justification for the simplified evaporation/condensation model

As we described in Section 3.1, we introduced several approximations in the evaporation/condensation model, in order to keep the model simple and easily reproducible. However, it is fair to ask to which extent these simplifications may affect the overall results. The two most serious approximations we made were (1) that $p_i^{\text{eq}} \propto f_i$ and (2) that p_i^{eq} does not depend on $f_{k \neq i}$. The evaporation/condensation theory reviewed in the appendices shows that neither are really correct. For Na and K we expect, from theory, more something like $p_i^{\text{eq}} \propto \sqrt{f_i}$, and the vapor pressures do influence each other.

In order to test whether these simplifications strongly affect the result (and thus make the result unreliable) we created also a model computer code where the equilibrium vapor pressures p_i^{eq} are recomputed at every time step using the full machinery described in the appendices. The only things we still keep constant are the activity coefficients, because they follow from the MELTS code, for which we do not have a version available at present that can be directly linked into our program. We compare the results for Na and K, for models F1 and F2. The results are shown in Fig. 7.

The results show that the simplified evaporation / condensation model does a very good job for Na and K compared to the more sophisticated model. The differences are presumably substantially smaller than many of the other model uncertainties, such as initial condition parameters. The simplified model is therefore, for these purposes, good enough.

3.4. High-temperature models

The fiducial models F1, \dots , F4 all start with a temperature of $T = 2000$ K. But what happens if the initial temperature is considerably higher? We reran all four models with an initial temperature of $T = 2300$ K. We name these models H1, \dots , H4. The results are shown in Fig. 8. It is seen that the main consequence is that the Na and K reach lower minima, and at the end more Na and K remains lost (in particular in models H2 and H4). The other elements do not experience much depletion at the end, but in models H1 and H3 the Fe and SiO are temporarily reduced after which they recondense again.

In type IAB chondrules one often finds low-Ca pyroxene rims (e.g. Hewins & Zanda 2012) which are interpreted as evidence for evaporation and recondensation of SiO. In the fiducial models (Fig. 4) the temperature is too low for appreciable SiO evaporation. But in the high temperature models (except for H4) a substantial evaporation and subsequent recondensation of SiO is observed, which might be consistent with such low-CA pyroxene rims, since the recondensing SiO may not have time to mix well with the cooling droplet. Fe evaporation usually accompanies SiO evaporation, but in our model we include only a single oxidation state of iron, so it would be premature to draw too strong conclusions from this.

It should be kept in mind that in these high temperature models (in particular in model H3) the original assumption that the radius of the chondrules does not change is no longer correct. With half the loss of mass, the radius is 20% smaller. Therefore these model results merely give a qualitative picture of what happens.

4. DISCUSSION AND CONCLUSION

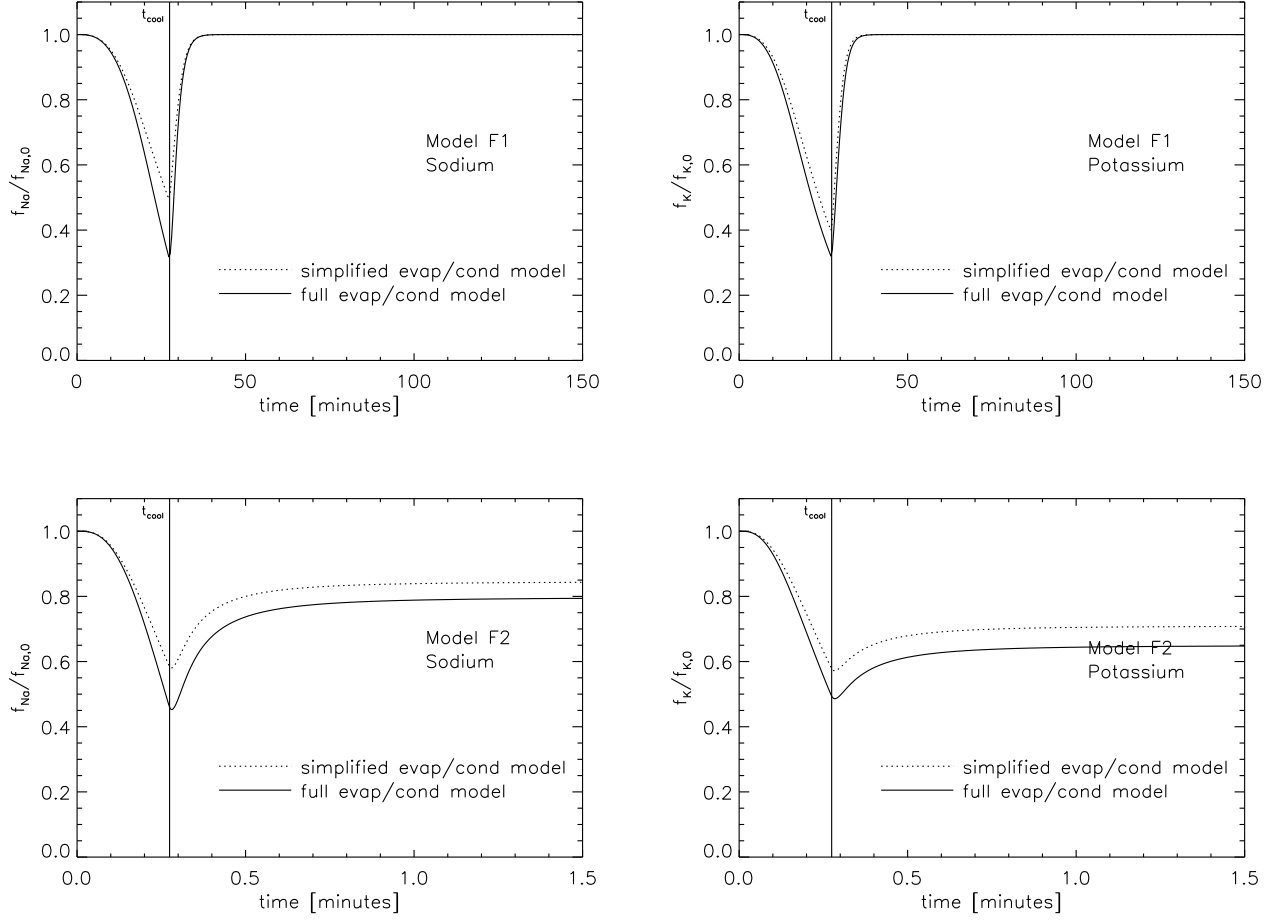


Figure 7. Comparison of the standard model with our simplified description of evaporation and condensation (dotted line) to a version of the model in which the equilibrium pressures are recalculated at every time step using the full machinery of evaporation/condensation described in the appendices (solid line). Top panels: Model F1 ($R_{\text{melt},0} = 1 \text{ km}$, $v_{\text{exp}} = 0.1 \text{ km/s}$), bottom panels: Model F2 ($R_{\text{melt},0} = 0.1 \text{ km}$, $v_{\text{exp}} = 1 \text{ km/s}$). Left panels: sodium, right panels: potassium.

In this paper we computed the degree of loss of volatile elements from chondrules formed in an impact-splash scenario. We use the simple spherically symmetric expanding chondrule cloud model of Paper I which gives us the chondrule density and temperature of the cloud as a function of radial coordinate inside the cloud and as a function of time. That model showed that initially the cloud stays at a constant temperature, but after a well-defined time starts to cool down due to radiative cooling. On the basis of this model we calculate how the volatile compounds Na_2O , K_2O , FeO , SiO_2 and MgO evaporate out of the molten chondrules but quickly reach their vapor equilibrium pressure, effectively halting the further evaporation. We find that shortly before the cloud starts to cool some elements (mainly Na and K) start to experience non-negligible losses from the chondrules (tens of percents). However, as the cooling sets in these elements usually rapidly recondense onto the chondrules.

The models of this paper show that volatile retention appears to be a natural consequence of the impact-splash origin scenario for chondrules. Since volatile retention is one of the critical observables in chondrules, our model calculations provide some further support for the impact splash scenario.

Depending on the parameters of the model (the cloud mass and expansion velocity) the recondensation can also, however, be incomplete (see e.g. model F2), leaving some signature of volatile loss in the chondrules. The fate of the remaining vapor is likely to recondense at a later stage onto the dust grains of the solar nebula. However, this typically happens only in the models with very rapid cooling (for model F2 this is 15 seconds), which appears to be inconsistent with typical chondrule textures. The models with many hours of cooling time appear to have complete recondensation. Since there exist in Nature chondrules with substantial Na and K depletion, as well as some chondrules with enhanced abundances, we speculate that more detailed physics of the expanding cloud has to be included, such as hydrodynamic flow of Na and K vapor through the cloud. Indeed, the present model assumes that the vapor stays inside the cloud, i.e. that there is no hydrodynamic escape. Also it is assumed that no nebular gas permeates into the cloud, at least not before the solidus temperature is reached. A future study will have to clarify if and how the results are affected by this aspect. One possible outcome could be that in addition to depleted abundances, the outer cloud regions may experience a surplus of volatiles because when volatiles

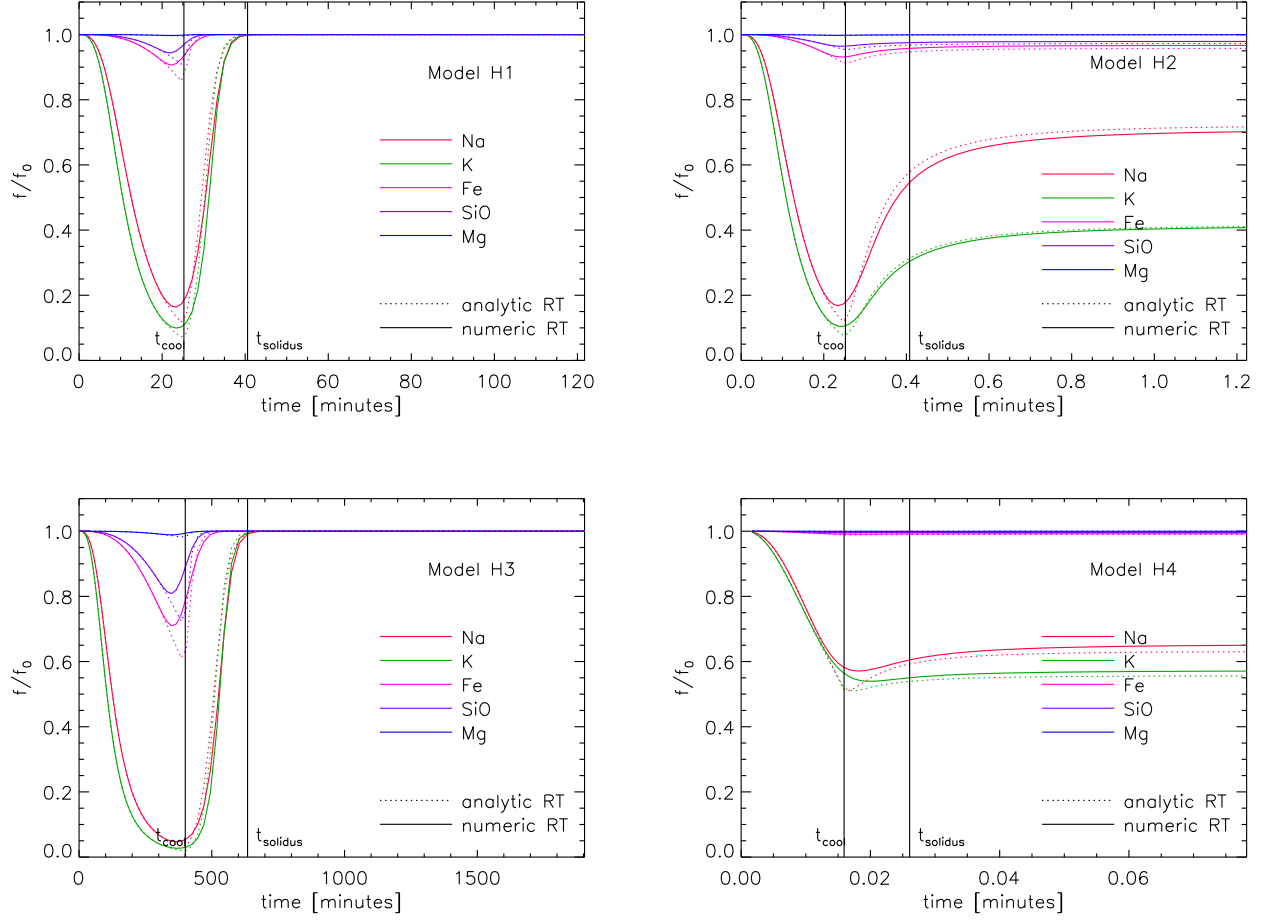


Figure 8. As Fig. 4, but now for a higher initial temperature: $T = 2300$ K. These models are marked as H1, H2, H3 and H4. For the rest the models are the same as the models F1, F2, F3 and F4 (Fig. 4).

from the cloud interior flow into the cooler cloud edge this could lead to accumulation of these elements.

Another issue that requires further study is whether all the recondensed vapor can quickly mix throughout the chondrule, to yield a homogeneous abundance, or whether the surface of the chondrules are expected to be enriched in volatile elements that recondensed in the late phases of the present model.

In spite of its simplicity, the predictions of our model appear to be consistent with the conclusions of Hewins, Zanda & Bendersky (2012) who find that there is evidence from Semarkona type II chondrules of evaporation and later recondensation of Na into these chondrules. This is indeed what our models show (see e.g. Fig. 4). These authors also write that “Type IIA chondrules lost more than half their Na and recondensation was incomplete” (consistent with our models F3 and F4), while “Type IIAB chondrules recovered most of theirs in their mesostases” (consistent with our models F1 and F2). In their section 4.3 they write “Even though the high concentrations of moderately volatile elements indicate that Type II chondrules may have formed in a high density region, there is still evidence of at least partially open system behavior.”, which is indeed what our model finds if the expansion and cooling is too quick for all the Na to recondense (models F3 and F4), thought that may

require too fast cooling to be consistent with textures.

Type I chondrules have low Fe and low Na content. Our model shows that Fe does not appreciably evaporate during the splash process, while Na does. It therefore seems that the low content of both elements in type I chondrules should be related to another process.

Type IAB chondrules show evidence of recondensation of SiO, which in our model would be consistent with higher initial temperatures.

Finally, it has long been thought that the chondrules from type CB (Bencubbin-like) chondrites originate from a hypervelocity impact (e.g. Krot et al. 2005). In addition to chondrules, these chondrites contain large amounts of metal spherules thought to have condensed out of the vapor phase. In fact, the Fe-Ni metal dominates by ~ 60 % the volume of these chondrites, and it is thought that the chondrules and the metal spherules formed during the same impact. Our model as it stands is too simple to simulate the conditions of this highly energetic event with high metal content. But the fact that they are highly depleted in Na and K and that they have only non-porphyritic textures without relic grains or rims (see Krot et al. 2005), suggests, in the context of our model and consistent with conclusions by other authors, that these formed in a very high-speed impact. Comparing to our model this scenario suggests high initial

temperature and a fairly small cloud (i.e. small M_{cloud}) with high plume expansion velocity v_{exp} . The high temperatures are probably necessary to create the Fe vapor, and the small, rapidly expanding cloud parameters ensure that the cooling is rapid and the Na and K vapor do not recondense. Our models H2 and H4 might go somewhat in that direction, but are probably not extreme enough. If we would stretch our model parameters too far, however, the underlying assumptions are broken and the model would be no longer valid. Qualitatively, however, it seems that the origin of CB chondrites as a result of an impact, as suggested by many authors in the past, fits well into our scenario.

In future studies it is important to study more realistic geometries. The nice thing of our simple spherically symmetric model is that many things can be quantitatively calculated quite easily. But it is clear that in reality the splashes from impacts of pre-molten bodies are not spherically expanding clouds. Smooth particle hydrodynamics (SPH) calculations may be required.

The evidence of chondrules being formed in high-pressure environments due to the retention of Na and K remains, however, subject to debate. Na and K may also re-enter at a much later stage, for instance due to contact with liquid water on the parent body, since Na and K are water-soluble. So it is important to study more detailed consequences of models of the kind presented in this paper. But the models so far seem to produce relatively robust results, i.e. not too strongly dependent on ill-constrained parameters. The partial evaporation and evaporation with a retention of all or most of the volatile elements Na and K is a very natural outcome of the model and requires no fine-tuning. That gives some confidence that impact splashes (be they due to hypervelocity impacts with jetting or due to lower speed impacts of pre-heated bodies) may be a natural explanation of the formation of chondrules.

Acknowledgements: We would like to thank Andreas Pack, Eric Gaidos, Knut Metzler, Alessandro Morbidelli, David Lundberg and Stephan Henke for useful discussions and feedback. We also thank the anonymous second referee for very useful input and suggestions.

This work has been supported by the Deutsche Forschungsgemeinschaft Schwerpunktprogramm (DFG SPP 1385) The first 10 Million Years of the Solar System – a Planetary Materials Approach (grants Du 414/12 and Du 414/14).

A.J. is grateful for the financial support from the European Research Council (ERC Starting Grant 278675-PEBBLE2PLANET), the Knut and Alice Wallenberg Foundation, and the Swedish Research Council (grant 2014-5775).

REFERENCES

- Alexander, C.M.O., 2001, *Meteoritics & Planetary Science* 36, 255
 Alexander, C.M.O., 2002, *Meteoritics and Planetary Science*, 37, 245
 Alexander, C.M.O., Grossman, J.N., Ebel, D.S., Ciesla, F.J., 2008, *Science*, 320, 1617
 Asphaug, E., Jutzi, M., Movshovitz, N., 2011, *Earth and Planetary Science Letters*, 308, 369
 Berman, R.G., 1988, *J. of Petrology*, Vol 29, 445
 Chase, M.W., 1998, *Journal of physical and chemical reference data*, Monograph No. 9
 Ciesla, F.J., Hood, L.L., 2002, *Icarus*, 158, 281
 Cuzzi, J., Alexander, C.M.O., 2006, *Nature*, 441, 483
 Desch, S.J., Connolly, H.C., 2002, *Meteoritics and Planetary Science*, 37, 183
 Dullemond, C.P., Stammer, S.M. and Johansen, A. 2014, *ApJ*, 794, 91 (Paper I)
 Eisenhour, D.D. & Buseck, P.R. 1995, *Icarus*, 117, 197211
 Fedkin, A.V., Grossman, L. and Ghiorso, M.S., 2006, *Geochimica et Cosmochimica Acta* 70, 206
 Fedkin, A.V., Grossman, L., Ciesla, F.J. & Simon, S.B. 2012, *Geochimica et Cosmochimica Acta*, 87, 81
 Fedkin, A.V. and Grossman, L., 2013, *Geochimica et Cosmochimica Acta* 112, 226250
 Ghiorso, M.S. & Sack, R.O., 1995, *Contributions to Mineralogy and Petrology*, 119, 197
 Gibbard, S. G., Levy, E. H. & Morfill, G. E. 1997, *Icarus*, 130, 517
 Hashimoto, A., 1983, *Geochemical Journal* 17, 111
 Hevey, P.J., Sanders, I.S., 2006, *Meteoritics and Planetary Science*, 41, 95
 Hewins, R.H. & Zanda, B. 2012, *Meteoritics & Planetary Science*, 47(7), 11201138
 Hewins, R.H., Zanda, B. & Bendersky, C., 2012, *Geochimica et Cosmochimica Acta*, 78, 1
 Hewins, R.H., Connolly, H.C., Lofgren, G.E. & Libourel, G., 2005, in *Chondrites and the Protoplanetary Disk*, 341, 286
 Holland, T.J.B. & Powell, R., 1998, *J. metamorphic Geol.*, 16, 309
 Hood, L.L., Horanyi, M., 1991, *Icarus*, 93, 259
 Horanyi, M., Morfill, G., Goertz, C.K. & Levy, E.H. 1995, *Icarus*, 114, 174185
 Hubbard, A., McNally, C. P. & Mac Low, M.-M. 2012, *ApJ*, 761, 58
 Jacquet, E., Gounelle, M. & Fromang, S. 2012, *Icarus*, 220, 162
 Johansen, A. & Youdin, A. 2007, *ApJ*, 662, 627641
 Johnson, B.C., Minton, D.A., Melosh, H. J. & Zuber, M.T. 2015, *Nature*, 517, 339341
 Kieffer, S., 1975, *Science*, 189, 333
 King, A.R. & Pringle, J.E. 2010, *MNRAS*, 404, 19031909
 Krot, A. N., Amelin, Y., Cassen, P. & Meibom, A. 2005, *Nature*, 436, 989992
 Morris, M. A. & Desch, S. J. 2010, *The Astrophysical Journal*, 722, 1474
 Sanders, I.S., Scott, E.R.D., 2012, *Meteoritics and Planetary Science*, 47, 2170
 Sanders, I.S., Taylor, G.J., 2005, *Chondrites and the Protoplanetary Disk*, 341, 915
 Shu, F. H., Shang, H., Gounelle, M., Glassgold, A. E., Lee, T. 2001, *ApJ*, 548, 1029
 Stammer, S.M. & Dullemond, C.P. 2014, *Icarus* 242, 1
 Urey, H.C., Craig, H. 1953, *Geochimica et Cosmochimica Acta*, 4, 36
 Yu, Y., Hewins, R.H., Alexander, C.M.O'D., and Wang, J., 2003 *Geochimica et Cosmochimica Acta*, 67, 773
 Zook, H.A., 1980, *Meteoritics*, 15, 390

APPENDIX

EQUILIBRIUM VAPOR PRESSURES FOR METAL OXIDE MELTS

For the calculation of time-dependent evaporation and condensation using the Hertz-Knudsen equation we need to know the equilibrium vapor pressures of the vapor species for a given temperature. These can be calculated from thermodynamic properties measured in the laboratory. In our case we are interested in evaporating molten rock. We will not consider the presence of H_2 gas nor an externally fixed oxygen pressure, but instead assume that the only

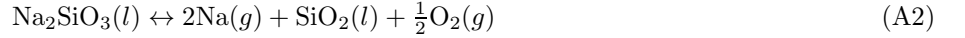
gas that is present is the evaporated vapor itself. For our model of an expanding cloud of lava droplets resulting from an impact this assumption is presumably reasonably valid. The procedure described here can, however, be easily generalized to the case of the presence of pre-existing gas. The procedure we discuss here is a simplified version of the procedure described in Fedkin et al. (2006).

Since the lava droplet is a mixture of different metal oxides, let us focus on one of them (our ‘metal oxide of interest’) with a mass fraction denoted by f . As an example we choose Na_2O , but the following discussion will also apply to other species. If the liquid would be an ideal fluid, one could use Raoult’s law which states that the equilibrium vapor pressure of the species interest equals f times the equilibrium vapor pressure of the pure species: $p^{\text{eq}} = f p^{\text{eq,pure}}$. One can regard this as saying that a fraction f of the surface of the melt is made out of our metal oxide of interest. This would greatly simplify the calculation of evaporation because we can then treat the evaporation of each species independent from the others.

Unfortunately for metal oxides the situation is more complex. First of all, molten metal oxides are usually far from ideal fluids. The linear relation $p^{\text{eq}} = f p^{\text{eq,pure}}$ does not necessarily hold. Instead, we must use the activity a rather than the mass fraction f , and the equilibrium vapor pressure will not necessarily be linear in a (nor in f). Secondly, the evaporating metal oxides tend to dissociate into its most stable gaseous atomic or molecular constituents. For instance, for Na_2O we have the following evaporation/condensation reaction:



where (l) means liquid and (g) means gas. Note that in the melt the metal can also be locked up in more complex forms. For Na this can be e.g. $\text{Na}_2\text{SiO}_3(l)$. The evaporation/condensation reaction then becomes



In either case there are more than one gas species coming out of the liquid, typically one being the metal and the other being oxygen. This means that in addition to the metal vapor pressure (in this case p_{Na}) we also have the oxygen vapor pressure p_{O_2} (which is equal to the oxygen fugacity since the vapor can be treated as an ideal gas). The metal equilibrium vapor pressure is then coupled to the oxygen vapor pressure because for each metal vapor particle also an oxygen vapor particle is ejected from the melt. Since all other evaporating metal species also depend on oxygen, the oxygen vapor pressure couples all metal vapor pressures to each other.

The equilibrium vapor pressure for the metal of interest can be computed from the equilibrium chemistry equation. Let us write the general form of the evaporation reaction as



where ‘M’ is the metal, ‘X’ is the combination of oxygen and possibly other elements that together with ‘M’ make up the compound, ‘Y’ is what remains of the liquid after the evaporation. If no remaining liquid substance ‘Y’ is involved we set $d = 0$. For reaction (A1) we would have $\text{M}=\text{‘Na’}$, $\text{X}=\text{‘O’}$, $c = 2$, $d = 0$ and $e = 0.5$. For reaction (A2) we have $\text{M}=\text{‘Na’}$, $\text{X}=\text{‘SiO}_3\text{’}$, $c = 2$, $d = 1$, $\text{Y}=\text{‘SiO}_2\text{’}$ and $e = 0.5$. The equilibrium partial pressure p_{M}^{eq} (in units of bar) of metal vapor species $\text{M}(g)$ can be calculated using the following equation:

$$K_{\text{evap}} = \frac{p_{\text{M}}^c p_{\text{O}_2}^e a_{\text{Y}}^d}{a_{\text{M}_c\text{X}}} \quad (\text{A4})$$

where K_{evap} is the equilibrium constant for the evaporation reaction, $p_{\text{M}} \equiv p_{\text{M}}^{\text{eq}}$ is the metal gas partial pressure (in units of bar), p_{O_2} is the oxygen gas partial pressure (in units of bar), $a_{\text{M}_c\text{X}}$ the activity of our metal oxide of interest in the fluid and (if present) a_{Y} the activity of the remaining liquid substance Y. Note that for convenience we will usually simply write p_{M} where actually the equilibrium vapor pressure p_{M}^{eq} is meant. The difference becomes only relevant in non-equilibrium cases. Note also that the reaction Eq. (A3) is not the most general one (for instance the evaporation of $\text{SiO}_2(l)$ into $\text{SiO}(g) + \frac{1}{2}\text{O}_2(g)$ is not strictly included, but the principle stays the same).

The equilibrium coefficient K_{evap} of the evaporation reaction can be computed by

$$K_{\text{evap}} = \exp\left(-\frac{\Delta_r G(T)}{RT}\right) \quad (\text{A5})$$

where R is the gas constant, T the temperature, $\Delta_r G(T)$ is the change of Gibbs free energy for the reaction and is given by

$$\Delta_r G(T) = c \Delta_f G_{\text{M}}(T) + e \Delta_f G_{\text{O}_2}(T) + d \Delta_f G_{\text{Y}}(T) - \Delta_f G_{\text{M}_c\text{X}}(T) \quad (\text{A6})$$

where for each species the $\Delta_f G(T)$ is the amount of Gibbs free energy needed to create that species from its elements in their most stable phase at that temperature (the reference phase). In appendix D the values of $\Delta_f G(T)$ for all the relevant species of this paper are given in the form of a polynomial fit to the laboratory data in the temperature range between 1400 and 2200 K.

We assume in our model that the only gas that is present is the vapor itself. If a single metal vapor species is dominating the oxygen production, then there is a simple linear relation between the metal vapor pressure p_{M} and the oxygen pressure p_{O_2} :

$$p_{\text{O}_2} = \frac{e}{c} p_{\text{M}} \quad (\text{A7})$$

Species	f_0	a_0	γ
Na ₂ O, Na ₂ SiO ₃	2.4213E-02	6.8057E-04	2.8108E-02
K ₂ O, KAlSiO ₄	2.9260E-03	4.7220E-03	1.6138E+00
FeO, Fe ₂ SiO ₄	1.4427E-01	1.1313E-01	7.8418E-01
SiO ₂ , SiO ₂	5.5589E-01	5.6297E-01	1.0127E+00
MgO, Mg ₂ SiO ₄	1.8866E-01	2.0890E-01	1.1073E+00
Al ₂ O ₃ , Al ₂ O ₃	4.8426E-02	6.1667E-03	1.2734E-01

Table 2

The composition f_0 and activities a_0 of the relevant constituents for composition 3 of Yu et al. (2003), where the Yu et al. mass fractions were normalized to unity (which leads to a small correction compared to the original Yu values). The first two columns list the compound of which the mass fraction f_0 is specified and the compound form for which the activity a_0 has been computed, respectively. The activities were computed with the MELTS code and are valid at 1850K. The activity coefficient γ is also computed at 1850 K but turns out to be fairly constant with temperature.

Using Eq. (A7) one can now eliminate p_{O_2} in Eq. (A4) in favor of p_M and, with the known value of K_{evap} (Eq. A5), solve for p_M . This then leads to

$$p_M = \left(K_{\text{evap}} \frac{a_{M_cX}}{a_Y^d} \left(\frac{c}{e} \right)^e \right)^{1/(e+c)} \quad (\text{A8})$$

With Eq. (A7) this gives then also p_{O_2} . For the more minor metal oxide vapor species one can solve Eq. (A4) now with the known value of p_{O_2} . If no single vapor species dominates, then Eq. (A7) becomes a summation over all contributing metals. An iteration procedure is then necessary, that eventually converges in the value of p_{O_2} .

Since we can evaluate K_{evap} for any given temperature, the above procedure gives an expression for p_M in terms of the activities of the metal oxide M_cX and (if applicable) of the residual substance Y . Typically, though, we specify as model parameter their mass fraction f , not their activity a . We need to translate f into a before we can make use of Eq. (A4). This can be done using the MELTS code¹ (Ghiorso & Sack 1995). We define the *activity coefficient* γ as

$$a = \gamma f \quad (\text{A9})$$

where f is the mass fraction² of the primary metal oxide, and a is the activity of the metal oxide species in the melt. For sodium this would be

$$a_{\text{Na}_2\text{SiO}_3} = \gamma f_{\text{Na}_2\text{O}} \quad (\text{A10})$$

This γ can be computed with MELTS for a specific composition (and thus a specific f). It is, however, not always guaranteed that γ is independent of f . The MELTS code gives the activity for the dominant compound involving the metal M in the melt (e.g. for sodium: Na₂SiO₃). Using equilibrium liquid \leftrightarrow liquid reactions the activity of the other compounds of the system can be easily calculated. For instance, using the equilibrium reaction



one gets $a_{\text{Na}_2\text{O}} = K_{\text{eq}} a_{\text{Na}_2\text{SiO}_3} / a_{\text{SiO}_2}$, with the equilibrium constant K_{eq} computed using Eq. (A5). The equilibrium vapor pressure p_{Na} computed for evaporation of Na₂SiO₃ will then be identical to that computed for the evaporation of Na₂O. We thus need to only compute a single evaporation channel.

EQUILIBRIUM VAPOR PRESSURES FOR NA, K, FE, SIO AND MG

Using the above procedure we now compute the equilibrium vapor pressure for sodium in the temperature range between 1400 K and 2200 K. For the melt composition we take composition 3 of Yu et al. 2003 (Geochimica et Cosmochimica Acta 67, 773). Using the MELTS code we compute the activities, and from that the activity coefficients. We define the activity coefficients as

$$\begin{aligned} \gamma_{\text{Na}_2\text{O}} &= a_{\text{Na}_2\text{SiO}_3} / f_{\text{Na}_2\text{O}}, & \gamma_{\text{K}_2\text{O}} &= a_{\text{KAlSiO}_4} / f_{\text{K}_2\text{O}}, \\ \gamma_{\text{FeO}} &= a_{\text{Fe}_2\text{SiO}_4} / f_{\text{FeO}}, & \gamma_{\text{SiO}_2} &= a_{\text{SiO}_2} / f_{\text{SiO}_2}, \\ \gamma_{\text{MgO}} &= a_{\text{Mg}_2\text{SiO}_4} / f_{\text{MgO}}, & \gamma_{\text{Al}_2\text{O}_3} &= a_{\text{Al}_2\text{O}_3} / f_{\text{Al}_2\text{O}_3} \end{aligned} \quad (\text{B1})$$

We find that for MgO, SiO₂, FeO and K₂O these coefficients are almost constant with temperature. For Al₂O₃ and Na₂O there is a mild variation with temperature, but we will, for convenience, also assume them to be constant with temperature, and take the value at 1850 K as representative. The mass fractions and the computed activities and activity coefficients are listed in Table 2.

¹ <http://melts.ofm-research.org>

² Conventionally the activity coefficient is defined in terms of the mole fraction, but for our purpose this definition is more convenient.

Species	q_0	q_1	q_2	q_3
Na	-3.3312E+01	3.2376E-02	-1.2206E-05	1.6938E-09
K	-3.2543E+01	2.6092E-02	-7.4375E-06	6.6993E-10
Fe	-5.6017E+01	5.7326E-02	-2.2493E-05	3.2120E-09
SiO	-6.2295E+01	5.9586E-02	-2.1152E-05	2.7561E-09
Mg	-6.1782E+01	5.7863E-02	-2.0728E-05	2.7294E-09
O ₂	-3.4994E+01	3.4414E-02	-1.3494E-05	1.9719E-09

Table 3

The resulting equilibrium vapor pressures for the composition of table 2 (Yu et al. 2003 composition 3) for the elements of interest (where all element pressures are coupled via the common oxygen pressure), expressed as a fitting function $\log^{10}(p^{\text{eq}}) = q_0 + q_1T + q_2T^2 + q_3T^3$ with the pressure in bar and temperature in Kelvin. The fit was done at temperatures 1400, 1700, 2000 and 2200 K. These fits correspond to the curves in Fig. 10.

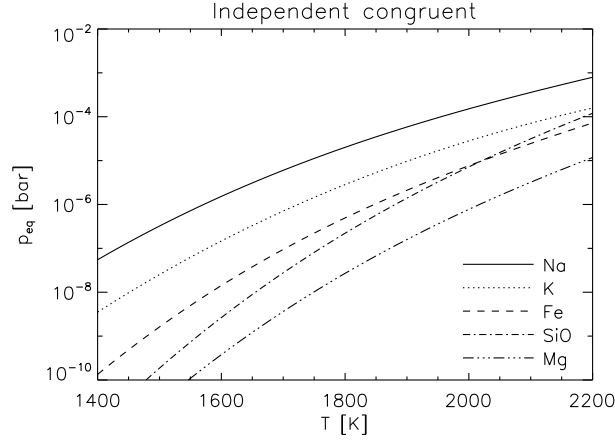
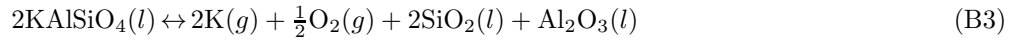


Figure 9. The equilibrium vapor pressures calculated from the model for Na, K, Fe, SiO and Mg for composition 1 from Yu et al. (2003). Each was calculated assuming a congruent oxygen pressure, assuming none of the other metal vapors to be present (i.e. $p_{\text{O}_2} = \frac{1}{4}p_{\text{Na}}$, $p_{\text{O}_2} = \frac{1}{4}p_{\text{K}}$, $p_{\text{O}_2} = \frac{1}{2}p_{\text{Fe}}$, $p_{\text{O}_2} = \frac{1}{2}p_{\text{SiO}}$, $p_{\text{O}_2} = \frac{1}{2}p_{\text{Mg}}$ respectively).

The evaporation reactions for the elements Na, K, Fe, SiO and Mg are then:



These reactions allow us to calculate the equilibrium vapor pressures of the elements for any given temperature T . We first calculate Gibbs free energy $\Delta_f G$ for each of the reactants and products using the polynomial fit of Eq. (D9) using the coefficients from Table 4. Then from Eq. (A6) we can calculate the change in the Gibbs free energy $\Delta_r G(T)$ for the reaction (where for the KAlSiO_4 reaction the equations have to be adapted accordingly). This then gives us the equilibrium coefficient K_{evap} using Eq. (A5). The activities of the liquid phases for our initial composition are obtained from Table 2. From Eq. (A4) we now obtain the value of the product of vapor pressures $p_{\text{M}}^c p_{\text{O}_2}^e$ (where we recall that c and e are defined in Eq. A3). For congruent evaporation for each metal species separately we can express p_{O_2} directly in terms of p_{M} using Eq. (A7). The solution of p_{M} is then found from Eq. (A8).

A more self-consistent approach is to calculate the vapor pressures for the coupled system. In this case we iterate over the oxygen pressure p_{O_2} , where after each iteration we recompute it according to

$$p_{\text{O}_2} = \frac{1}{4}p_{\text{Na}} + \frac{1}{4}p_{\text{K}} + \frac{1}{2}p_{\text{Fe}} + \frac{1}{2}p_{\text{SiO}} + \frac{1}{2}p_{\text{Mg}} \quad (\text{B7})$$

where we recall that we assume that there is no nebular gas inside the expanding cloud of molten droplets, and hence the oxygen pressure is entirely due to the evaporated material.

In principle we should also consider the formation of a whole plethora of diatomic molecules (such as $\text{MgO}(g)$) in the gas phase, which would add to the vapor pressure (see e.g. Fedkin et al. 2006). But these pressures are low and we will ignore them.

For the above mentioned composition 3 of Yu et al. (2003) the resulting equilibrium pressures for congruent evaporation are shown in Fig. 9 for each species independently, and in Fig. 10 for the coupled system. In Table 3 these results are given in terms of the coefficients of a third-order polynomial fit.

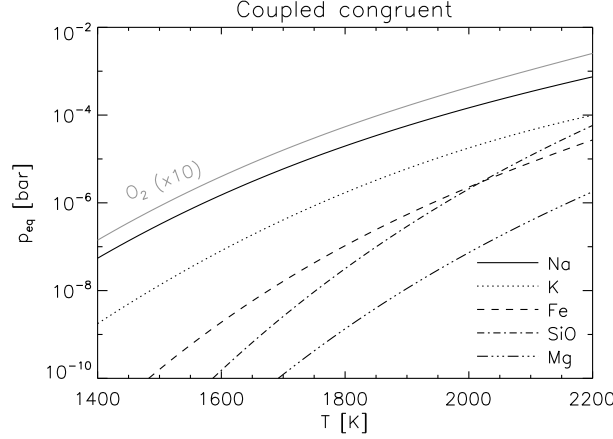


Figure 10. The equilibrium vapor pressures calculated from the model for Na, K, Fe, SiO and Mg for composition 1 from Yu et al. (2003). They are all coupled by all contributing to the oxygen pressure according to Eq. (B7). Note that the oxygen pressure is shown at 10x its value, to avoid overcrowding of the figure.

These results show that for this mixture (with a roughly 10x larger K abundance than typically found in chondrules) the K pressure dominates. For abundances of K more in line with typical chondrule values, the Na pressure typically dominates. In the coupled figure one sees that the high oxygen pressure set by K pushes the vapor pressures of Na, Fe and Mg down compared to their independent values.

From the above analysis we see that the sodium equilibrium vapor pressure is proportional to $\sqrt{a_{\text{Na}_2\text{SiO}_3}}$ for constant p_{O_2} and proportional to $a_{\text{Na}_2\text{SiO}_3}^{0.4}$ for congruent evaporation (i.e. $p_{\text{O}_2} = 0.25 p_{\text{Na}}$). Since the MELTS code finds that the activity coefficient is approximately constant with the mass fraction $f_{\text{Na}_2\text{O}}$ (at least for mass fractions not higher than a few percent), it follows that $p_{\text{Na}}^{\text{eq}} \propto \sqrt{f_{\text{Na}_2\text{O}}}$ for constant p_{O_2} and $p_{\text{Na}}^{\text{eq}} \propto f_{\text{Na}_2\text{O}}^{0.4}$ for congruent evaporation. This is very different from Raoult's law, and this has consequences for the non-equilibrium behavior of evaporation, as we shall discuss in Section C.

Note that the square-root behavior of the sodium vapor pressure (for fixed p_{O_2}) is due to the fact that each unit of Na_2SiO_3 (or each unit of Na_2O) in the liquid phase releases two units of Na vapor. Alexander (2001) instead considers the basic unit in the liquid to be $\text{NaO}_{1/2}$. This makes (at least for fixed p_{O_2}) the sodium vapor pressure again linear in the activity. This paradox is solved by realizing that the activity a is not necessarily linearly proportional to the mass fraction f . For the Na_2O versus $\text{NaO}_{1/2}$ paradox one can see this from the simple neutral chemical “reaction” $\text{Na}_2\text{O} \leftrightarrow 2\text{NaO}_{1/2}$, which has $K_{\text{eq}} = 1 = a_{\text{NaO}_{1/2}}^2 / a_{\text{Na}_2\text{O}}$ showing that $a_{\text{NaO}_{1/2}} = \sqrt{a_{\text{Na}_2\text{O}}}$. So if, as the MELTS code seems to indicate to some approximation, $a_{\text{Na}_2\text{O}} \propto f_{\text{Na}_2\text{O}}$, then it follows that $a_{\text{NaO}_{1/2}} \propto \sqrt{f_{\text{Na}_2\text{O}}}$. Therefore both viewpoints lead to the same behavior.

TIME-DEPENDENT EVAPORATION/CONDENSATION OF METAL OXIDE MELTS

The Hertz-Knudsen equation and the definition of equilibrium vapor pressures under non-equilibrium conditions

Let us now consider a drop of liquid that is time-dependently evaporating. This process is governed by the Hertz-Knudsen equation:

$$\begin{aligned}
 J &= J_{\text{evap}} - J_{\text{cond}} \\
 &= v_{\text{vap}} \left(\frac{\alpha_{\text{evap}} p_{\text{vap}}^{\text{eq}}}{kT} - \alpha_{\text{cond}} n_{\text{vap}} \right) \\
 &\equiv v_{\text{vap}} \frac{\alpha_{\text{evap}} p_{\text{vap}}^{\text{eq}} - \alpha_{\text{cond}} p_{\text{vap}}}{kT}
 \end{aligned} \tag{C1}$$

where J_{evap} is the number of molecules per second per cm^2 leaving the surface of the drop, J_{cond} is the number of molecules per second per cm^2 condensing onto the surface of the drop, J is the net evaporation rate, k is the Boltzmann constant, T the temperature in Kelvin, $p_{\text{vap}}^{\text{eq}}$ is the equilibrium vapor pressure (this time in units of dyne/ cm^2), n_{vap} is the number density of the vapor molecules in the gas phase (in units of cm^{-3}), $p_{\text{vap}} \equiv n_{\text{vap}} kT$ is the vapor pressure, $v_{\text{vap}} \equiv \sqrt{kT/2\pi m}$ is the average projected molecular velocity, m is the molecular mass. The coefficients α_{evap} and α_{cond} are the evaporation and condensation coefficients, where α_{evap} is the probability that a molecule leaving the surface will remain in the vapor phase and not get bounced back onto the surface by molecular collisions, while α_{evap} is the probability that a molecule that hits the surface will stick to the surface and not bounce back into the gas.

To assure that thermodynamic equilibrium is guaranteed (i.e. that $J = 0$ when $p_{\text{vap}} = p_{\text{vap}}^{\text{eq}}$), we must have $\alpha_{\text{evap}} =$

α_{cond} under conditions near equilibrium. Far from equilibrium, however, we could have $\alpha_{\text{evap}} \neq \alpha_{\text{cond}}$. For the classical evaporation process of molecules that do not dissociate upon evaporation (e.g. evaporation of water or methane) one can usually say that $\alpha_{\text{evap}} = \alpha_{\text{cond}}$ and that $p_{\text{vap}}^{\text{eq}}$ is independent of the conditions in the gas above the liquid surface. That means then that the evaporation rate J_{evap} is also independent on those conditions and saturation is reached simply when the actual vapor pressure p_{vap} has increased to the level of the equilibrium vapor pressure $p_{\text{vap}}^{\text{eq}}(T)$.

For evaporation of metal oxide melts, where the evaporating metals are accompanied by evaporating oxygen (i.e. dissociation upon evaporation), the situation is more complex. It is still described by the Hertz-Knudsen equation, this time for each of the vapor constituents separately (e.g. for Na_2O we would write Eq. C1 for Na vapor and for O_2 separately, but clearly the equations are linked via stoichiometry, because we must have $J_{\text{O}_2} = 0.25 J_{\text{Na}}$), but now the equilibrium vapor pressure, and therefore J_{evap} , is no longer independent of the conditions in the gas phase above the liquid surface. According to Eq. (A4), if we increase the oxygen pressure p_{O_2} in the gas above the liquid surface, then the equilibrium vapor pressure for the metal vapor p_{M}^{eq} decreases, and therefore typically also its evaporation rate $J_{\text{evap,M}}$.

Far away from equilibrium it becomes somewhat ambiguous how to define the equilibrium vapor pressure. One way is to fix the oxygen pressure p_{O_2} to the current value and compute the p_{M}^{eq} using Eq. (A4) for that given value of p_{O_2} . Another way is to assume congruent evaporation in which the oxygen pressure is solved along with those of the metal vapor pressures ($p_{\text{O}_2}^{\text{eq}} = \sum_i (e_i/c_i) p_{\text{M}_i}^{\text{eq}}$), plus perhaps some background oxygen pressure if present. Both definitions lead to different equilibrium vapor pressures (compare Fig. 9 with Fig. 10). Yet, the evaporation rate J_{M} , being a measureable quantity, should not be dependent on the choice of definition. The different behavior of $\alpha_{\text{evap,M}}$ and $\alpha_{\text{cond,M}}$ under these different definitions ensures that the results are nevertheless identical.

Exactly what the values of $\alpha_{\text{evap,M}}$ and $\alpha_{\text{cond,M}}$ are and how they change as a function of p_{M} , p_{O_2} (and other constituents of the gas above the liquid surface) is not a simple question to answer. It requires laboratory experiments under all the conditions of interest. The complexity of all of this, in particular far away from equilibrium conditions, makes the numerical modeling of strongly non-equilibrium time-dependent evaporation/condensation problems somewhat uncertain, unless the conditions remain close to those measured in the laboratory.

Typically laboratory measurements are made of evaporation rates at low vapor pressures, i.e. $p_{\text{M}} \ll p_{\text{M}}^{\text{eq}}$. These experiments are done either at given oxygen pressures or into near vacuum. In some cases also other gases are present (e.g. H_2 gas or air at a given pressure). For some metals these additional gases can affect the evaporation and condensation rates substantially. For instance, Yu et al. (2003) show that when H_2 gas is present, the evaporation rates of Na are increased. From these measured values of $J_{\text{evap,M}} = J_{\text{evap,M}}^{\text{lab}}$, and for a given choice of definition of the equilibrium vapor pressure, one can compute the value of $\alpha_{\text{evap,M}}$.

Time-dependent vapor loss from molten metal oxides

When a small molten lava droplet loses some of its constituents (say the metal oxide M_cX) through the evaporation reaction



into a *finite volume* V , the concentration of that constituent declines and the vapor pressure of the corresponding metal gas increases. As a result, the evaporation rate drops and the condensation rate rises. Let us study the time-dependent loss of metal oxide M_cX (let us call this ‘the volatile’ from here on) from the droplet including both these effects. Define the mass weighted abundance f of this volatile inside the lava droplet:

$$m_{\text{volatile}} = f m_{\text{drop}} \quad (\text{C3})$$

where m_{volatile} is the amount of gram of volatile that is still remaining inside the droplet. We measure f in terms of the evaporating part of this metal oxide, e.g. for the evaporation of Na_2SiO_3 we measure the mass fraction of Na_2O , because the rest is, upon evaporation, left behind as SiO_2 . We assume that the droplet is completely liquid, so that the volatile is always perfectly mixed within the droplet, and no concentration gradients form toward the surface. If we ignore the difference in material density between the volatile and the rest of the droplet, then the fraction of the surface that consists of volatile particles is again f , meaning that f , together with the known saturation pressure for that volatile, indeed determines the evaporation rate.

If we now have a finite volume V around the droplet into which the vapor can escape, then the vapor pressure p_{M} and the volatile mass fraction f are related via:

$$\frac{m_{\text{vap}} V p_{\text{M}}}{kT} = (f_0 - f) m_{\text{drop}} \quad (\text{C4})$$

where f_0 is the initial mass fraction of the volatile in the drop before evaporation and

$$m_{\text{vap}} = m_{\text{M}} + \frac{e}{c} m_{\text{O}_2} \quad (\text{C5})$$

is the mass of the metal atom plus the corresponding mass of the oxygen molecules that join in the evaporation/condensation process. We have used the ideal gas law $p_{\text{M}} = n_{\text{M}} kT$ (with n_{M} the number density of metal M vapor atoms in the gas phase) combined with the total mass of vapor (metal and oxygen) in the volume $m_{\text{vap}} V n_{\text{M}}$.

Although the vapor pressure p_M and the volatile mass fraction in the droplet f are related through Eq. (C4), in the following we will still use p_M and f separately for clarity.

The mass loss (or gain) rate of the droplet through evaporation (or condensation) of the volatile metal oxide given by

$$\frac{d(m_{\text{volatile}})}{dt} \equiv \frac{d(fm_{\text{drop}})}{dt} \equiv m_{\text{drop}} \frac{df}{dt} = -4\pi a_{\text{drop}}^2 J_M m_{\text{vap}} \quad (\text{C6})$$

where a_{drop} is the radius of the droplet, J_M is the evaporation rate of the metal M in units of number of vapor particles per surface area.

The evaporation rate of metal M can be expressed as a function of f and p_M using the Hertz-Knudsen equation Eq. (C1), expressed here as

$$J_M(f, p_M, p_{\text{O}_2}, T) = \frac{\alpha_{\text{evap},M} p_M^{\text{eq}}(f, p_{\text{O}_2}, T) - \alpha_{\text{cond},M} p_M}{\sqrt{2\pi m_M k T}} \quad (\text{C7})$$

where the evaporation and condensation coefficients $\alpha_{\text{evap},M}$ and $\alpha_{\text{cond},M}$ are functions of f , p_M , p_{O_2} and T . In principle all these functions can be non-linear functions, as described in Sections A and C.1. The functional form of the equilibrium vapor pressure $p_M^{\text{eq}}(f, p_{\text{O}_2})$, once we fix its definition (see Section C.1), can be computed using the math of Section C.1 and a model of the activity a_{M_cX} as a function of the mass fraction f (e.g. the MELTS model). Typically this is a non-linear behavior.

The functional form of the $\alpha_{\text{evap},M}(f, p_M, p_{\text{O}_2})$ and $\alpha_{\text{cond},M}(f, p_M, p_{\text{O}_2})$ coefficients is not well known, due to limited experimental data, and generally requires a simplified model or formula that is calibrated against the experimental data that is available. There are numerous papers that describe the results of such efforts (e.g. Alexander 2001, 2002; Fedkin et al. 2006, 2012, 2013 and many more). Typically a constant value is inferred by comparing the measured evaporation rate J at low pressures with $\alpha_{\text{evap},M} p_M^{\text{eq}}$, and then it is typically assumed that $\alpha_{\text{cond},M} = \alpha_{\text{evap},M}$. One can use these values for modelling, as long as one remains close to the conditions of the experiments against which these values were inferred. As shown above, however, for conditions far from these, things become uncertain.

Fedkin et al. (2006) have done a careful study of several of these experiments, and determined the α coefficients for Na, K, Mg, Fe and SiO. Rather than doing our own fits to the experiments we use the values reported in that paper.

THERMODYNAMIC DATA

For most solid compounds we use the thermodynamic data from Ghiorso & Sack (1995), based on the Berman model³ (Berman 1988). We also use the NIST JANAF tables⁴ (Chase 1998) for several other compounds not in the Ghiorso & Sack or Berman models, as well as for the gas-phase.

Using thermodynamic data from different databases together in the same model requires special care, because the definitions of the zero-enthalpy are often different. For convenience of the reader we review here how the databases are combined.

It is the international convention to define the formation enthalpy $\Delta_f H^0(298)$ (in units of $\text{JK}^{-1}\text{mol}^{-1}$) of a certain compound from its elements at the reference temperature $T_r = 298.15$ K and at the reference pressure of 1 bar. A compound is defined as a substance made of multiple elements, such as SiO_2 . The elements are defined as the pure substances made of the elements or of the molecules defined as the reference molecule. For the compound SiO_2 these are Si and O_2 (by convention the reference oxygen is molecular oxygen, while for the metals the reference is usually the pure metal: Fe, Mg, Na, Si etc). The formation enthalpy of the elements in their reference state are therefore by definition $\Delta_f H^0(298) = 0$.

In the NIST-JANAF database tables the 6th column gives the temperature-dependent formation enthalpy $\Delta_f H^0(T)$. This is defined as the formation enthalpy at temperature T from the most stable form of the elements *at the same temperature*. This means that for a compound this function is given by

$$\begin{aligned} \Delta_f^{\text{jnf}} H^0(T) &= \Delta_f H^0(298) + [H^0(T) - H^0(298)]_{\text{compound}} \\ &\quad - \sum_i [H^0(T) - H^0(298)]_{\text{elem},i} \end{aligned} \quad (\text{D1})$$

(Chase 1998), “jnf” stands for NIST-JANAF, and $H^0(T) - H^0(298)$ is listed in the 5th column of the tables. The formation Gibbs function using the same definition is then

$$\begin{aligned} \Delta_f^{\text{jnf}} G^0(T) &= \Delta_f^{\text{jnf}} H^0(T) - [TS^0(T)]_{\text{compound}} \\ &\quad + \sum_i [TS^0(T)]_{\text{elem},i} \end{aligned} \quad (\text{D2})$$

(Chase 1998). One can verify that this is equal to column 7 of the NIST-JANAF database. For the elements in their reference state the $\Delta_f H^0(T)$ and $\Delta_f G^0(T)$ are, by definition, zero at *all* temperatures.

³ <http://ctserver.ofm-research.org/ThermoDataSets/Berman.php>

⁴ <http://kinetics.nist.gov/janaf/>

In the Berman (1988) paper, as well as in the Holland & Powell (1998) paper and the Ghiorso & Sack (1995) paper, the $\Delta_f H^0(298)$, the entropy $S^0(298)$ and volume for 1 mole $V^0(298)$ are given at the reference temperature. To compute $H^0(T) - H^0(298)$ one must integrate

$$H^0(T) - H^0(298) = \int_{298.15}^T C_P(T') dT' \quad (D3)$$

where $C_P(T)$ is the specific heat. An analytically integrable (polynomial) fitting formula for $C_p(T)$ is given in Berman (1988) and a different one in Holland & Powell (1998). The coefficients of these fitting formulae are listed in those papers. Berman (1988), Ghiorso & Sack (1995) and Holland & Powell (1998) define the formation enthalpy $\Delta_f^{\text{ber}} H^0(T)$ of a compound at temperature T from its elements at the reference temperature $T_r = 298.15$:

$$\Delta_f^{\text{ber}} H^0(T) = \Delta_f H^0(298) + [H^0(T) - H^0(298)] \quad (D4)$$

Let us, from now on, refer to the ‘Berman definition’ whenever we mean ‘Berman, Ghiorso & Sack and Holland & Powell definition’. The NIST-JANAF and Berman definitions of the formation enthalpy are thus related as follows:

$$\Delta_f^{\text{jnf}} H^0(T) = \Delta_f^{\text{ber}} H^0(T) - \sum_i [H^0(T) - H^0(298)]_{\text{elem},i} \quad (D5)$$

In the Berman definition the formation Gibbs energy $\Delta_f^{\text{ber}} G^0(T)$ is also defined with respect to the elements at 298.15 K:

$$\begin{aligned} \Delta_f^{\text{ber}} G^0(T) &= \Delta_f^{\text{ber}} H^0(T) - TS^0(T) \\ &= \Delta_f G^0(298) + [H^0(T) - H^0(298)] - T [S^0(T) - S^0(298)] \end{aligned} \quad (D6)$$

where $S^0(T)$ is found from $S^0(298)$ through

$$S^0(T) - S^0(298) = \int_{298.15}^T \frac{C_P(T')}{T'} dT' \quad (D7)$$

which is also analytically integrable using the above mentioned fitting polynomials. Note that in Berman’s definition, neither $\Delta_f^{\text{ber}} H^0(T)$ nor $\Delta_f^{\text{ber}} G^0(T)$ are zero for temperatures $T \neq 298.15\text{K}$. The NIST-JANAF and Berman definition of the formation Gibbs function are related as follows:

$$\Delta_f^{\text{jnf}} G^0(T) = \Delta_f^{\text{ber}} G^0(T) - \sum_i [H^0(T) - H^0(298)]_{\text{elem},i} + \sum_i [TS^0(T)]_{\text{elem},i} \quad (D8)$$

Of course the actual numbers are slightly different due to different sources of the data and different approximations.

For the computation of the equilibrium coefficient of a chemical reaction (in our case evaporation) one can either use $\Delta_f^{\text{jnf}} G^0(T)$ or $\Delta_f^{\text{ber}} G^0(T)$, as long as all substances involved use the same definition, because the sum over the elements drops out of the equation. However, when using data from both databases one must first convert all data to the same convention.

In this paper we adopt the NIST-JANAF definitions. For convenience we make a third-order polynomial fit to the dimensionless form of the Gibbs formation energy $\Delta_f^{\text{jnf}} G^0(T)/RT$ for several elements and compounds of interest:

$$\frac{\Delta_f^{\text{jnf}} G^0(T)}{RT} = a + bT + cT^2 + dT^3 \quad (D9)$$

where T is in Kelvin. The coefficients a , b , c and d are obtained by fitting Eq. (D9) through the values at 1400, 1700, 2000 and 2200 Kelvin. These fits are good enough for the purpose of this paper within the temperature range 1400 - 2200 K, but are not to be used beyond this range since polynomial fits are known to quickly diverge when used beyond their fitting range. The results are listed in Table 4.

Species	a	b	c	d	Ref
SiO (g)	-1.0517E+01	-2.3503E-02	1.7198E-05	-3.3390E-09	JANAF
Mg (g)	0.0000E+00	0.0000E+00	0.0000E+00	0.0000E+00	JANAF
Fe (g)	9.6481E+01	-9.7974E-02	3.7134E-05	-5.1464E-09	JANAF
Na (g)	0.0000E+00	0.0000E+00	0.0000E+00	0.0000E+00	JANAF
K (g)	0.0000E+00	0.0000E+00	0.0000E+00	0.0000E+00	JANAF
O ₂ (g)	0.0000E+00	0.0000E+00	0.0000E+00	0.0000E+00	JANAF
Al ₂ O ₃ (s/l)	-4.1984E+02	3.8554E-01	-1.4237E-04	1.9508E-08	B+GS
SiO ₂ (s/l)	-1.9367E+02	1.5332E-01	-4.7042E-05	5.2773E-09	B
MgO (s/l)	-1.7563E+02	1.6901E-01	-6.2570E-05	8.5805E-09	JANAF
Mg ₂ SiO ₄ (s/l)	-5.5777E+02	4.9903E-01	-1.7357E-04	2.2387E-08	B+GS
MgSiO ₃ (s/l)	-3.8799E+02	3.4433E-01	-1.1902E-04	1.5120E-08	JANAF
FeO (s/l)	-7.4390E+01	7.6634E-02	-3.1269E-05	4.6587E-09	JANAF
Fe ₂ O ₃ (s)	-1.7353E+02	1.5434E-01	-4.9512E-05	5.4840E-09	B+GS
Fe ₃ O ₄ (s)	-2.5146E+02	2.3429E-01	-8.4549E-05	1.1470E-08	JANAF
Fe ₂ SiO ₄ (s/l)	-3.3765E+02	3.0061E-01	-1.0743E-04	1.4317E-08	B+GS
FeSiO ₃ (s)	-2.6207E+02	2.1903E-01	-7.1972E-05	8.8483E-09	B
Na ₂ O (s/l)	-1.1988E+02	1.2844E-01	-4.8364E-05	6.6846E-09	JANAF
Na ₂ SiO ₃ (s/l)	-3.8065E+02	3.4204E-01	-1.1879E-04	1.5348E-08	B+GS
K ₂ O (s/l)	-1.1465E+02	1.3492E-01	-5.4470E-05	8.0269E-09	JANAF
KAlSiO ₄ (s/l)	-4.9643E+02	4.2598E-01	-1.4312E-04	1.7709E-08	B+GS

Table 4

The coefficients for the polynomial fit to the dimensionless Gibbs free energy $\Delta_f^{\text{inf}} G(T)/RT$ (Eq. D9) in the temperature range between 1400 and 2200 K. The reference states of the elements are not listed because for them $\Delta_f^{\text{inf}} G(T)/RT = 0$ by definition. The coefficients were fitted to the data from the NIST-JANAF database (those with ref JANAF), or the Berman (1998) model (ref B) or the Berman model for the solid phase and the Ghiorso & Sack (1995) model for the liquid phase (ref B+GS). Note that for the solid phase Ghiorso & Sack (1995) also use the Berman model. All the data in this table are in the same definition (the JANAF definition) and are thus mutually consistent. However, no guarantee is given that the polynomial fits we show here are accurate enough for other applications than the simplified model of this paper.